nature structural & molecular biology

Crystal structure, conformational fixation and entry-related interactions of mature ligand-free HIV-1 Env

Young Do Kwon[1,18], Marie Pancera[1,18], Priyamvada Acharya[1,18], Ivelin S Georgiev[1,18], Emma T Crooks[2], Jason Gorman[1], M Gordon Joyce[1], Miklos Guttman[3], Xiaochu Ma[4], Sandeep Narpala[1], Cinque Soto[1], Daniel S Terry[5], Yongping Yang[1], Tongqing Zhou[1], Goran Ahlsen[6,7], Robert T Bailer[1], Michael Chambers[1], Gwo-Yu Chuang[1], Nicole A Doria-Rose[1], Aliaksandr Druz[1], Mark A Hallen[1,8], Adam Harned[9], Tatsiana Kirys[1], Mark K Louder[1], Sijy O'Dell[1], Gilad Ofek[1], Keiko Osawa[2], Madhu Prabhakaran[1], Mallika Sastry[1], Guillaume B E Stewart-Jones[1], Jonathan Stuckey[1], Paul V Thomas[1], Tishina Tittley[1], Constance Williams[10], Baoshan Zhang[1], Hong Zhao[5], Zhou Zhou[5], Bruce R Donald[8,11,12], Lawrence K Lee[13], Susan Zolla-Pazner[10,14], Ulrich Baxa[9], Arne Schön[15], Ernesto Freire[15], Lawrence Shapiro[1,6], Kelly K Lee[3], James Arthos[16], James B Munro[4,17], Scott C Blanchard[5], Walther Mothes[4], James M Binley[2], Adrian B McDermott[1], John R Mascola[1] & Peter D Kwong[1]

As the sole viral antigen on the HIV-1–virion surface, trimeric Env is a focus of vaccine efforts. Here we present the structure of the ligand-free HIV-1–Env trimer, fix its conformation and determine its receptor interactions. Epitope analyses revealed trimeric ligand-free Env to be structurally compatible with broadly neutralizing antibodies but not poorly neutralizing ones. We coupled these compatibility considerations with binding antigenicity to engineer conformationally fixed Envs, including a 201C 433C (DS) variant specifically recognized by broadly neutralizing antibodies. DS-Env retained nanomolar affinity for the CD4 receptor, with which it formed an asymmetric intermediate: a closed trimer bound by a single CD4 without the typical antigenic hallmarks of CD4 induction. Antigenicity-guided structural design can thus be used both to delineate mechanism and to fix conformation, with DS-Env trimers in virus-like-particle and soluble formats providing a new generation of vaccine antigens.

© 2015 Nature America, Inc. All rights reserved.

HIV type 1 (HIV-1) uses multiple mechanisms to evade the immune system, and these have stymied the development of an effective vaccine[1–3]. One mechanism—conformational masking[4]—hides the vulnerable shape of the trimeric envelope (Env) recognized by broadly neutralizing antibodies via structural rearrangements that expose immunodominant epitopes recognized by non-neutralizing or poorly neutralizing ('ineffective') antibodies[5,6]. The upshot is that virus infection and Env immunization both elicit abundant production of Env-directed antibodies with little neutralization capacity[7–9]. A potential solution is to determine the structure of the vulnerable Env conformation and to use this structural information and protein design to stabilize or to fix the vulnerable shape.

Definition of the structure of trimeric HIV-1 Env has been accomplished at increasing resolution by crystallography and cryo-EM[10–14]. These studies have culminated in atomic-level structures of antibody-bound forms of a near-native trimer mimic, named BG505 SOSIP.664, for HIV-1 strain (BG505)[15] and stabilizing mutations (SOSIP.664)[16–18]. However, bound antibodies can influence conformation. Structures of the Env gp120 subunit, for example, can differ substantially when ligand free[19] or when bound to different antibodies[3,6,20–24]. HIV-1 Env, moreover, is a type 1 fusion machine, which uses structural rearrangements to drive the merging of virus and host-cell membranes during entry (reviewed in ref. 25). Substantial prefusion-to-postfusion conformational changes accompany this process[14,26,27], and single-molecule fluorescence resonance transfer (smFRET) analysis has indicated that prefusion ligand-free Env on infectious virions undergoes transitions among at least three different conformations[28].

[1]Vaccine Research Center, National Institute of Allergy and Infectious Diseases, National Institutes of Health, Bethesda, Maryland, USA. [2]San Diego Biomedical Research Institute, San Diego, California, USA. [3]Department of Medicinal Chemistry, University of Washington, Seattle, Washington, USA. [4]Department of Microbial Pathogenesis, Yale University School of Medicine, New Haven, Connecticut, USA. [5]Department of Physiology and Biophysics, Weill Cornell Medical College of Cornell University, New York, New York, USA. [6]Department of Biochemistry & Molecular Biophysics, Columbia University, New York, New York, USA. [7]Department of Systems Biology, Columbia University, New York, New York, USA. [8]Department of Biochemistry, Duke University Medical Center, Durham, North Carolina, USA. [9]Electron Microscopy Laboratory, Cancer Research Technology Program, Leidos Biomedical Research, Frederick National Laboratory for Cancer Research, Frederick, Maryland, USA. [10]New York University School of Medicine, New York, New York, USA. [11]Department of Chemistry, Duke University, Durham, North Carolina, USA. [12]Department of Computer Science, Duke University, Durham, North Carolina, USA. [13]Structural and Computational Biology Division, Victor Chang Cardiac Research Institute, Darlinghurst, New South Wales, Australia. [14]New York Veterans Affairs Harbor Healthcare System, New York, New York, USA. [15]Department of Biology, Johns Hopkins University, Baltimore, Maryland, USA. [16]Laboratory of Immunoregulation, National Institute of Allergy and Infectious Diseases, National Institutes of Health, Bethesda, Maryland, USA. [17]Department of Molecular Biology and Microbiology, Tufts University School of Medicine, Boston, Massachusetts, USA. [18]These authors contributed equally to this work. Correspondence should be addressed to P.D.K. (pdkwong@nih.gov).

Received 1 April; accepted 29 May; published online 22 June 2015; doi:10.1038/nsmb.3051

When a viral antigen can assume multiple conformations, which is the 'right' conformation to fix? Clues from smFRET[28] and hydrogen/deuterium exchange (HDX) experiments[29] have suggested that a single dominant conformation, the mature prefusion closed state, is recognized by broadly neutralizing antibodies. Here we set out not only to fix HIV-1 Env in its vulnerable shape but also to determine the appropriate conformation to fix. We layered antigenic considerations—for both structure and binding—onto structure-based design. To provide a basis for the analysis, we determined the crystal structure of the ligand-free HIV-1–Env trimer and analyzed its structural compatibility with epitopes defined in previously determined antibody-bound Env structures. We coupled structural compatibility with binding measurements to identify both an 'appropriate target conformation' and an 'appropriate target antigenicity' and used antigenicity-guided structural design to fix the desired target shape. We then examined the functional and antigenic consequences of conformational fixation. Functional analysis revealed that HIV-1 Env transitions through an asymmetric intermediate, and antigenic analysis indicated improved specificity for broadly neutralizing antibodies. Together, our results provide a foundation by which to understand ligand-free HIV-1–Env trimer: its structure, its entry-related mechanistic interactions and its conformational fixation as a means to overcome conformational masking.

RESULTS

Structure and properties of ligand-free HIV-1–Env trimer

To obtain the structure of mature ligand-free HIV-1 Env, we used a sparse-matrix approach[30] to crystallize an endoglycosidase H–treated BG505 SOSIP.664 trimer from a PEG 400–PEG 3350 precipitant mixture[31]. Diffraction data extended to 3.3 Å but were anisotropic with a nominal resolution of 3.7 Å (**Table 1**). Because of the lower resolution, we were careful with crystallographic *B* factors; refinement without *B* factors did not reduce R_{free} to below 33%, whereas refinement[32] with group *B* factor and translation-libration-screw motions yielded R_{work}/R_{free} of 26.6%/28.5% (**Fig. 1**, **Table 1** and **Supplementary Figs. 1** and **2**). The resulting *B* factors correlated strongly with real-space correlation (**Supplementary Table 1**), thus suggesting a reflection of prefusion coordinate mobility.

To provide insight into the physical characteristics of ligand-free HIV-1 Env, we analyzed residue and surface properties including sequence entropy, atomic mobility, hydrophobicity, polarity and surface accessibility (**Fig. 1** and **Supplementary Figs. 1** and **2**). Of these, Cα differences between separate subunit structures and the ligand-free trimer showed moderate correlation with *B* factors (**Supplementary Tables 1** and **2**). When only the gp41 subunit was considered, the correlation increased (P <0.0001; **Fig. 1b**). Thus, gp41 regions of ligand-free trimeric Env that are structurally similar in the separate subunit context exhibit lower *B* factors, increased hydrophobicity, reduced surface accessibility and reduced sequence variation: these regions include the nascent α7 coiled coil, which underpins the internal coiled coil of the postfusion six-helix bundle. In contrast,

Table 1 Data collection and refinement statistics

	Ligand-free HIV-1 BG505 SOSIP.664
Data collection	
Space group	$P6_3$
Cell constants	
a, *b*, *c* (Å)	107.6, 107.6, 103.3
α, β, γ (°)	90, 90, 120
Resolution (Å)	50.0–3.30 (3.42–3.30)[a]
R_{merge}	9.4 (42.5)
$I / \sigma I$	14.3 (1.3)
Completeness (%)	68.3 (14.6)
Redundancy	5.2 (2.2)
Refinement	
Resolution (Å)	35.3–3.3
Unique reflections	6,434
R_{work} / R_{free} (%)	26.6 / 28.5
No. atoms	
Protein	4,518
Carbohydrate	338
B factors (Å^2)	
Protein	93.8
Carbohydrate	124.7
r.m.s. deviations	
Bond lengths (Å)	0.004
Bond angles (°)	1.147

[a]Values in parentheses are for highest-resolution shell; the highest-resolution shell for which data were 50% complete with I/σ greater than two was 3.91–3.72 Å. We therefore consider this structure to have a nominal resolution of 3.72 Å. One crystal was used for data measurements.

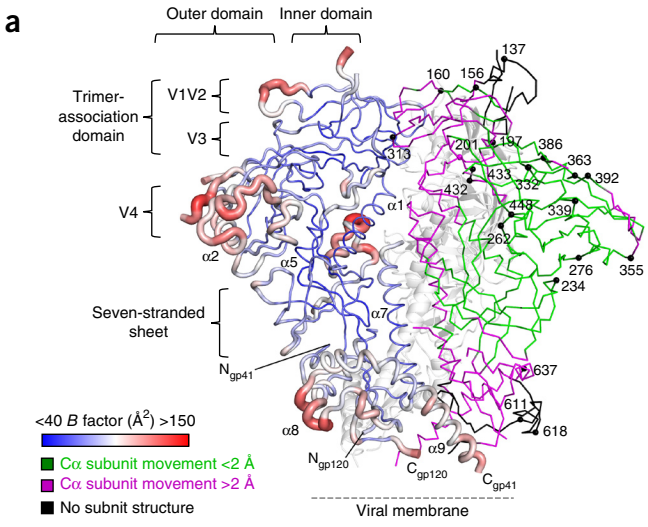

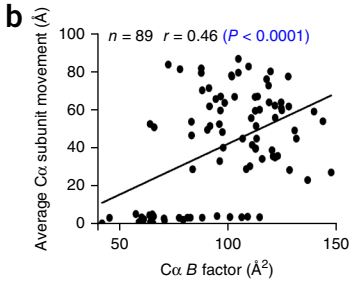

c

Virus	Correlation (*r*)	*P* value (*P*)
HIV	0.56	9.86×10^{-7}
Influenza	0.69	$<2.20 \times 10^{-16}$
RSV	0.46	$<2.20 \times 10^{-16}$

Figure 1 Crystal structure of ligand-free HIV-1–Env trimer and conformational changes related to individual subunit structures and virus entry. (**a**) Structure of the ligand-free BG505 SOSIP.664 trimer. The left gp120–gp41 protomer is shown in *B*-factor putty representation; the right protomer in Cα-backbone representation, colored according to average Cα distance between ligand-free Env and previously determined Env subunit structures, with residues highlighted with black spheres numbered; and the third protomer in gray cartoon. (**b**) Plot of prefusion Env *B* factors versus Cα subunit movement (full listing of correlations and *P* values in **Supplementary Table 1**). (**c**) Correlations and *P* values for prefusion *B* factors of type 1 fusion machines versus prefusion-to-postfusion movement of the fusion subunit (subunit pictorials and correlation graphs in **Supplementary Fig. 3**). *P* values in **b** and **c** were obtained by two-tailed Student's *t* test (*n* defined in **Supplementary Fig. 3**).

© 2015 Nature America, Inc. All rights reserved.

gp41 regions that differ in the separate subunit context, such as the α8 and α9 helices, displayed higher *B* factors, increased polarity and higher surface accessibility in the prefusion closed state.

One explanation for these results is that gp41 residue-level properties associated with prefusion mobility presage or predict regions that move between prefusion and postfusion states. Indeed, prefusion *B* factors correlated strongly with gp41 movement between prefusion and postfusion states (**Fig. 1c**). Relevant to this, we also observed that prefusion *B* factors of the fusion subunit from influenza virus (HA2) and respiratory syncytial virus (F1) correlated with prefusion-to-postfusion movement (**Fig. 1c** and **Supplementary Fig. 3**). Thus, clues to viral entry–related conformational change can be found in the ligand-free prefusion structures of Env, with residues of the fusion subunits in these type 1 fusion machines

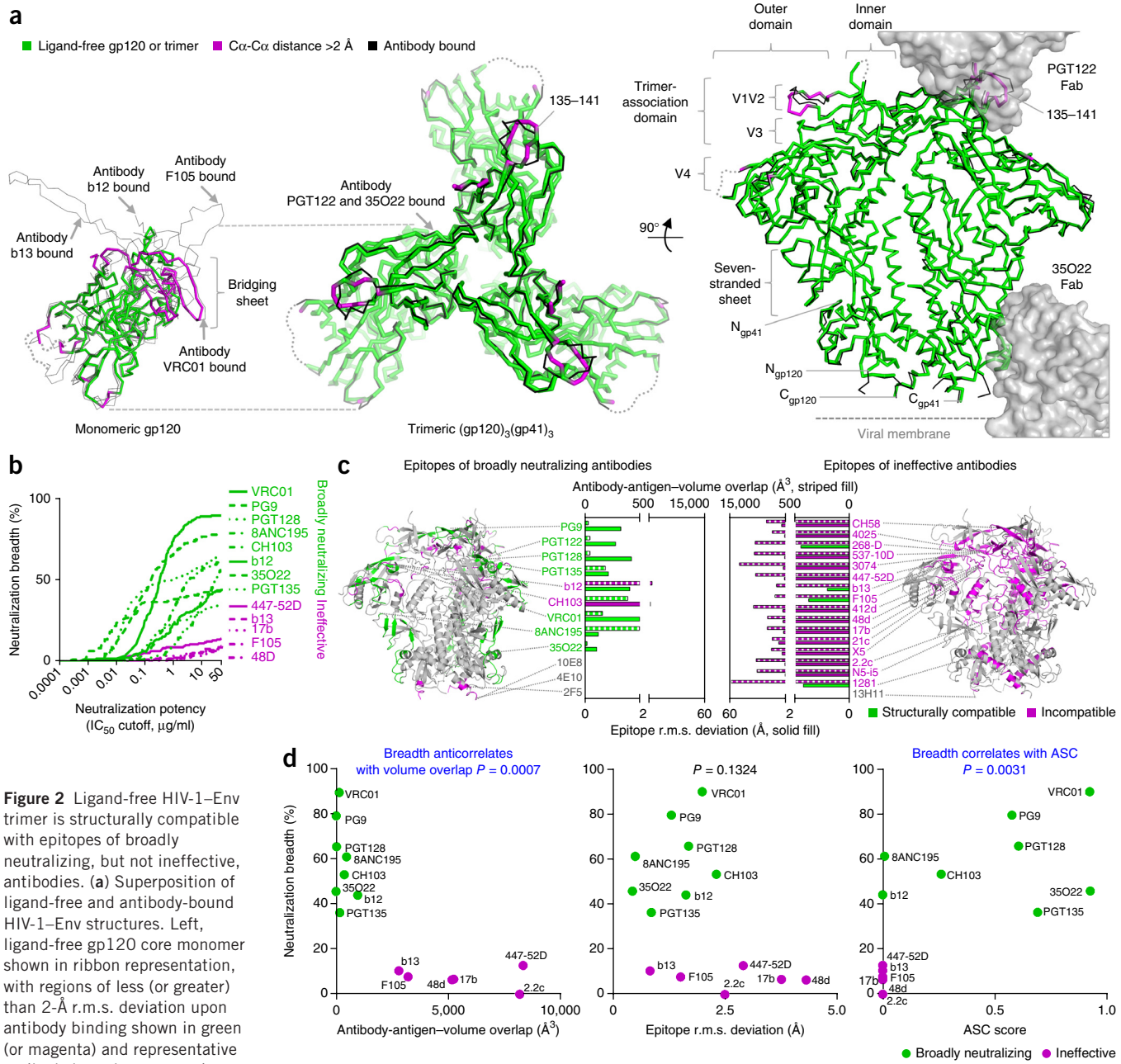

Figure 2 Ligand-free HIV-1–Env trimer is structurally compatible with epitopes of broadly neutralizing, but not ineffective, antibodies. (**a**) Superposition of ligand-free and antibody-bound HIV-1–Env structures. Left, ligand-free gp120 core monomer shown in ribbon representation, with regions of less (or greater) than 2-Å r.m.s. deviation upon antibody binding shown in green (or magenta) and representative antibody-bound structures in gray. Middle and right, ligand-free and antibody-bound HIV-1–Env trimers. At right, antibodies PGT122 and 35O22 are shown in gray semitransparent surface, and the rear protomer has been removed for clarity. r.m.s. deviations are reported in **Supplementary Table 7**. (**b**) Breadth-potency plot of broadly neutralizing (green) and ineffective (magenta) antibodies on a diverse 170 HIV-1–isolate panel. (**c**) Structural compatibility of ligand-free trimer by antibody epitope. The ligand-free Env structure is displayed as Cα ribbon, with antibody-epitope residues colored green (structurally compatible) or magenta (incompatible) or gray for nonepitope regions. r.m.s. deviation (solid fill) and volume overlap (striped fill) with the indicated antibody–Env complexes are shown in bar graph, with two linear scales split at r.m.s. deviation and antibody-antigen–volume overlap cutoffs of 2 and 500 Å^3, respectively; bars below the respective cutoffs are colored green and magenta otherwise. Antibody labels are colored green if the epitope is structurally compatible, magenta if incompatible and gray if not present in the structure. (**d**) Ligand-free-trimer structural compatibility versus antibody breadth. Volume overlap (left), r.m.s. deviation (middle) and antigenic structural compatibility (ASC) score (right), plotted versus antibody breadth on a diverse 170 HIV-1–isolate panel (pictorial representations in **Supplementary Fig. 5**). *P* values for Spearman correlations provided ($n = 14$ antibodies).

© 2015 Nature America, Inc. All rights reserved.

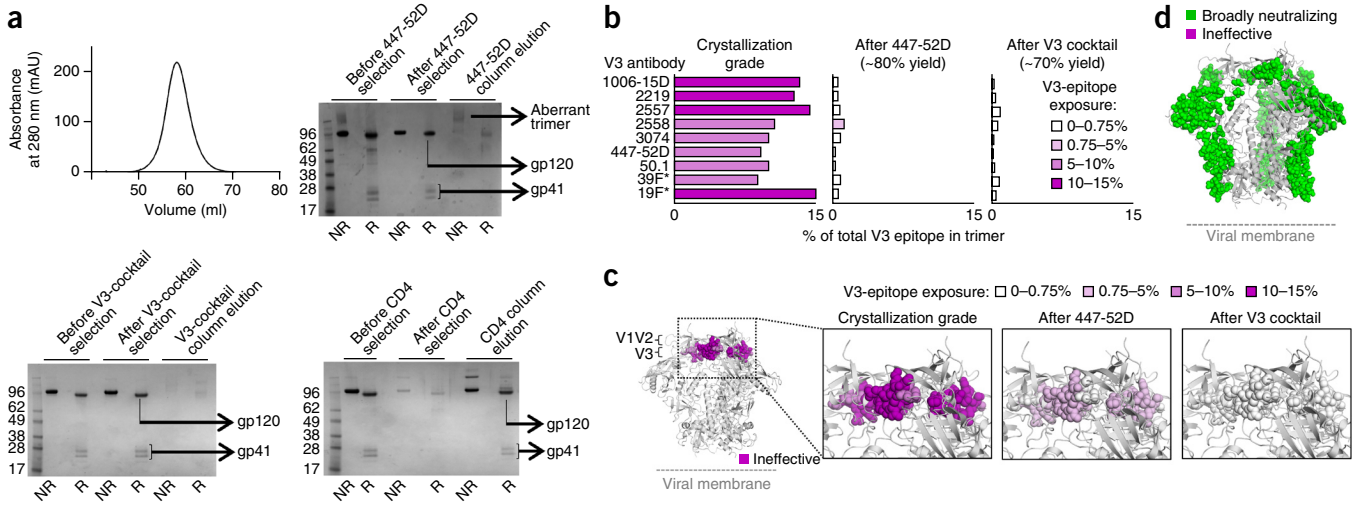

Figure 3 Structural compatibility–guided negative selection and an appropriate target antigenicity. (**a**) Top left, size-exclusion chromatography profile of crystallization-grade SOSIP before negative selection. Top right and bottom, SDS-PAGE analyses of negative selection: first with antibody 447-52D, next with a cocktail of V3 antibodies and third by CD4. NR, nonreducing conditions, R, reducing conditions. (**b**) V3-epitope exposure on BG505 SOSIP.664, quantified by SPR on a panel of V3 antibodies and displayed as percentage of total V3 epitope exposed upon CD4 triggering. Asterisks indicate that V3 epitopes for antibodies 39F and 19b have not been structurally defined. (**c**) V3 antigenicity for all structurally defined antibodies in **b**, mapped onto epitope atoms in the structure of the ligand-free Env trimer. (**d**) Appropriate target antigenicity. Binding antigenicity is displayed on the ligand-free Env trimer with epitope atoms with high-affinity trimer binding to broadly neutralizing antibodies in green and to ineffective antibodies in magenta.

poised on a mobility gradient to undergo the requisite conformational rearrangements required for entry.

Structural compatibility and appropriate target conformation

In addition to facilitating virus entry, HIV-1 Env functions to evade the humoral immune response, a function in which glycan shielding and conformational change are critical. In the refined ligand-free Env structure, we observed electron density corresponding to single protein-proximal *N*-acetyl glucosamine residues at all sites of N-linked glycosylation, except at residues 197, 262 and 332 (with Env numbering following standard HXB2 convention)[33], for which we observed additional monosaccharide residues, or at residue 137, which was mostly disordered (**Supplementary Fig. 4**). Overall, despite differences in glycosylation and lattice packing (**Supplementary Fig. 4**), the structure of the ligand-free trimer assumed a closed conformation, which was highly similar to that of antibody-bound trimers[12–14], especially the PGT122-35O22–bound trimer[14], with which it had an r.m.s. deviation in Cα positions of less than 1 Å, substantially lower than observed with monomeric gp120 (**Fig. 2a**).

To determine the appropriateness of the ligand-free closed trimer as a vaccine template, i.e., structural specificity for broadly neutralizing antibodies and incompatibility with non-neutralizing or poorly neutralizing antibodies, we first sought to categorize antibodies according to their functional efficacy (**Fig. 2b**). We defined broadly neutralizing antibodies as those with greater than 35% breadth on a diverse panel of 170 isolates and defined ineffective antibodies as those with less than 15% breadth. (For an isolate to be considered sensitive in this breadth analysis, we used a cutoff for antibody half-maximal inhibitory concentration (IC_{50}) of <50 μg/ml). Antibodies b12 (ref. 34), 35O22 (ref. 35) and PGT135 (ref. 36) were close to the cutoff for the broadly neutralizing category. Some antibodies showed clade-specific breadth, for example, V3-directed 447-52D[37], which neutralizes over 20% of clade B isolates. However, we nonetheless classified 447-52D as ineffective because its overall breadth was only 12% (**Supplementary Table 3**). We then analyzed the ligand-free closed structure for its structural compatibility with antibody epitopes—most determined structurally in the context of antibody-bound subunit or antibody-bound peptide—on the basis of two measures: antibody-volume overlap and epitope r.m.s. deviation (**Fig. 2c** and **Supplementary Fig. 5**). Antibody-volume overlap, which involves the superposition of epitopes in the ligand-free trimer and the antibody-bound context (**Supplementary Fig. 5**), was strongly anticorrelated with neutralization breadth ($P = 0.0007$; **Fig. 2d**). Epitope r.m.s. deviation, which compares epitope structural differences in the ligand-free trimer and the antibody-bound context, varied with breadth but did not achieve statistical significance. An antigenic structural-compatibility score (ASC), which combined both overlap and r.m.s. deviation, did achieve significance ($P = 0.0031$; **Fig. 2d**).

The ligand-free closed structure was compatible with the epitopes for all broadly neutralizing antibodies, except those of the membrane-proximal external region, which recognize epitopes C terminal to residue 664, and those of antibodies b12 (ref. 21) and CH103 (ref. 38), with CH103 exceeding a 2-Å threshold of epitope similarity and b12 exceeding a volume threshold of 500 $Å^3$ (**Fig. 2d**). In light of the poor correlation of epitope r.m.s. deviation with neutralization breadth (**Fig. 2d**), the r.m.s. deviation threshold was somewhat arbitrary. Nonetheless, the specific incompatibility of these moderately effective CD4-binding-site antibodies suggests that movement of residues of the CD4-binding site could occur relative to the ligand-free closed trimer; indeed, induced trimer movements have been observed for b12 (which binds poorly to the BG505 SOSIP.664 trimer[18]) by EM[10] and HDX[29]. By contrast, none of the epitopes for non-neutralizing or poorly neutralizing antibodies were structurally compatible with the ligand-free closed structure (**Fig. 2d**). These results indicate that the ligand-free closed trimer is structurally specific for neutralizing antibodies and thus is in an appropriate target conformation for immunogen design.

Appropriate target antigenicity for an Env-vaccine antigen

Structural specificity, as measured by epitope compatibility, is only one of the requirements of an appropriate vaccine template, and antigenic specificity, as measured by antibody binding, is also crucial.

© 2015 Nature America, Inc. All rights reserved.

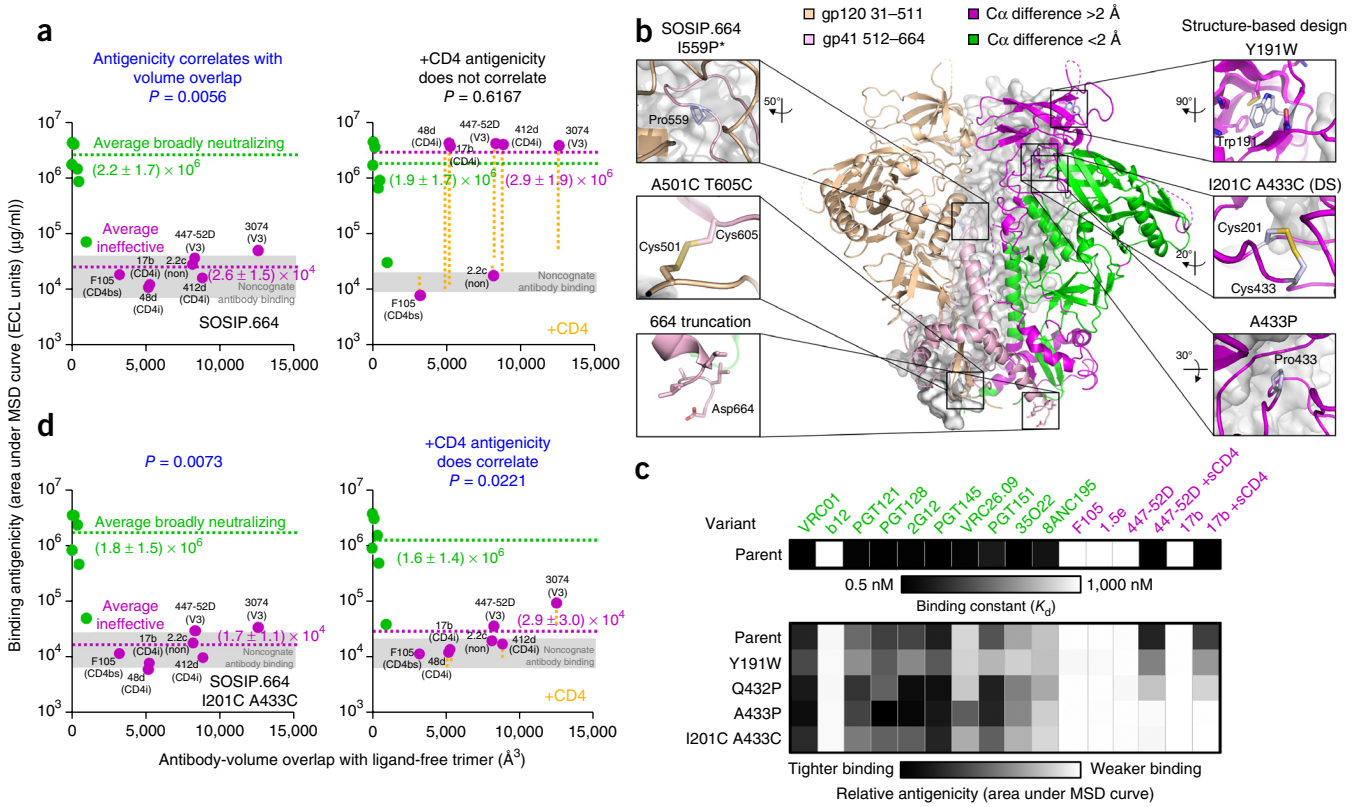

Figure 4 CD4-induced changes in antigenicity and conformational fixation of ligand-free HIV-1 Env. (**a**) BG505 SOSIP.664 ligand-free structural compatibility versus binding antigenicity, in the absence (left) and presence (right) of CD4, as measured by MSD-ECLIA. Antibodies are displayed in green (broadly neutralizing) and magenta (ineffective), and the average binding of each is provided. Ineffective antibodies are labeled (CD4bs, CD4-binding site; CD4i, CD4 induced; non, non-neutralizing; V3, V3-loop directed). The change in binding to ineffective antibodies in the presence of CD4 is shown as a yellow dotted line. *P* values for Spearman correlations are provided ($n = 13$ antibodies). Binding levels for noncognate antibodies (against influenza and RSV) lie within the gray shaded areas. (**b**) Conformational fixation of HIV-1–Env trimer. The central image depicts the ligand-free BG505 SOSIP.664 HIV-1–Env trimer, with two protomers shown in cartoon representation, one colored by domains (gp120 in wheat and gp41 in light pink) and a second colored by r.m.s. deviation distance between ligand-free trimer and subunit structures of CD4-bound gp120 and postfusion gp41 (green if less than 2 Å; magenta if more than 2 Å). A third protomer is shown in gray. Insets, atomic-level details. Asterisk denotes residue 559, which is disordered in the ligand-free structure. (**c**) Binding antigenicity of BG505 SOSIP.664 variants. Heat map showing binding of BG505 SOSIP.664 and variants that stabilized the ligand-free closed state to a panel of antibodies. (**d**) Ligand-free-trimer structural compatibility versus BG505 SOSIP.664 201C 433C binding antigenicity in the absence (left) and presence (right) of CD4, with antibodies and average binding in green (broadly neutralizing) and magenta (ineffective), as in **a**. (ELISA, Octet and Biacore data in **Supplementary Data Set 2** and **Supplementary Tables 5** and **6**).

The BG505 SOSIP.664 has previously been shown to be antigenically specific for broadly neutralizing antibodies, though binding to weakly neutralizing antibodies such as those directed to the V3 loop has been reported[18].

Our structural-compatibility analysis indicated that V3 antibodies are incompatible with the ligand-free closed state (**Fig. 2c**), suggesting that the binding of BG505 SOSIP.664 to V3 antibodies might not be intrinsic to the closed conformation of the SOSIP.664 construct but may instead be an artifact of alternative folding. Indeed, we found that negative selection[39] by weakly neutralizing V3-directed antibodies substantially reduced V3 antibody binding to BG505 SOSIP.664 (**Fig. 3a** and **Supplementary Data Set 1**); when we tested recognition on a panel of V3-directed antibodies, negative selection by 447-52D and by a V3-antibody cocktail reduced recognition by V3-directed antibodies to a level similar to that observed for noncognate antibody binding (**Fig. 3b**,**c**). We also tested CD4-negative selection but did not observe a substantial non-CD4-binding subportion of Env trimers. Together, these results indicated that an appropriate target antigenicity for an Env-vaccine antigen (**Fig. 3d**) would involve no recognition by ineffective antibodies (including those directed at the V3 region), while maintaining recognition of broadly neutralizing antibodies (except those with moderate neutralization, directed at the CD4-binding site).

CD4 triggering and conformational stabilization

Even after V3-antibody negative selection, CD4 triggering could efficiently expose V3 epitopes[40], recognized by antibodies such as 447-52D[41], 3074 (ref. 42) and others, as well as bridging-sheet epitopes[20], recognized by antibodies such as 17b[43] (**Fig. 4a** and **Supplementary Data Sets 2** and **3**). Thus, although structural compatibility (and neutralization breadth) generally correlated with antibody binding, this correlation was lost in the presence of CD4 (**Fig. 4a** and **Supplementary Data Set 2**). Notably, CD4 triggered BG505 SOSIP.664 recognition of ineffective antibodies so that their average binding was tighter than that of the broadly neutralizing ones (**Fig. 4a**). Such CD4 triggering makes BG505 SOSIP.664 less desirable as an immunogen: in primates, it would bind CD4 *in vivo* and would thus be predicted to elicit production of primarily ineffective antibodies against highly immunogenic CD4-induced epitopes.

© 2015 Nature America, Inc. All rights reserved.

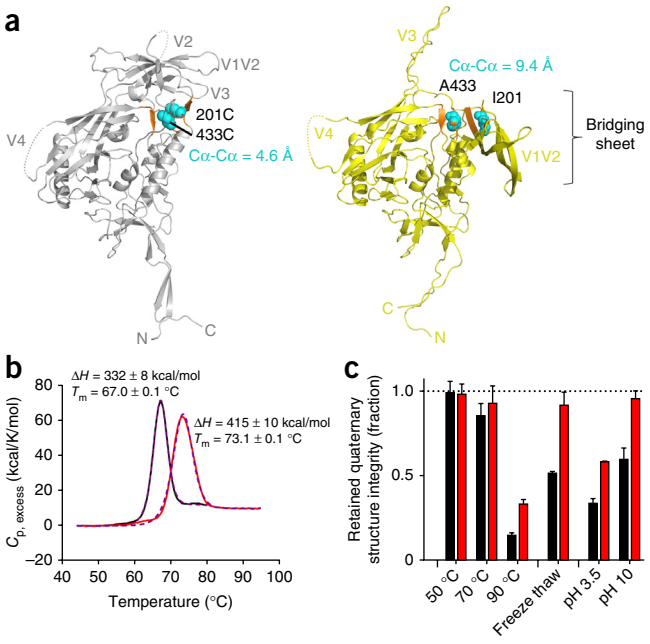

Figure 5 Atomic-level models and physical stability of ligand-free 201C 433C mutant (DS-SOSIP). (**a**) Atomic-level models of residues 201 and 433 in ligand-free prefusion closed state (gray) and CD4-bound state (yellow). Ribbon representations of the two structures are shown, with residues that make up the bridging sheet in the CD4-bound conformation colored orange, residues 201 and 433 colored cyan and shown as spheres and the 201-433 Cα distance indicated. Variable loops are labeled. (Monomeric CD4-bound conformation modeled from PDB 2B4C[6], 3U4E[59] and 3JWD[14]). (**b**) Thermostability of the DS-SOSIP, assessed by differential scanning calorimetry. Raw data are shown in solid line (black for BG505 SOSIP.664 and red for DS-SOSIP), with corresponding curves from the fit shown in purple dashed lines. Melting temperature (T_m) values and error were obtained from the fit. (**c**) Physical stability of trimeric DS-SOSIP, as determined by the quaternary-specific antibody VRC26.09 after 60 min of incubation at physical extremes or after ten freeze-thaw cycles. Color scheme as in **b**. Error bars, s.e.m. of two technical replicates.

To fix the ligand-free closed state and to prevent CD4 triggering, we analyzed regions of the ligand-free closed structure that moved upon CD4 binding and identified cavity-filling hydrophobic substitutions, side chain pairs capable of forming disulfide bonds and positions where the introduction of a proline would be compatible with only the ligand-free closed structure of Env but not its receptor-bound conformation (**Fig. 4b**). We engineered these substitutions into BG505 SOSIP.664, coexpressed them with furin in a 96-well transfection format[44] and assessed supernatants on an antigenic panel comprising broadly neutralizing antibodies PGT122 (ref. 36) and VRC01 (ref. 45), quaternary-specific broadly neutralizing antibodies PGT145 (ref. 36) and CAP256-VRC26.09 (ref. 46) and poorly neutralizing antibodies F105 (ref. 47) and 17b (ref. 43), with the latter tested alone and in the presence of CD4. In total, we tested 124 constructs (**Supplementary Table 4**). We purified and analyzed promising constructs for gp120-gp41 cleavage and oligomeric heterogeneity (**Supplementary Fig. 6**) and used mesoscale-discovery electrochemiluminescence immunoassay (MSD-ECLIA) to determine recognition on a more comprehensive panel of HIV-1–reactive antibodies (**Fig. 4c**, **Supplementary Data Set 2** and **Supplementary Tables 5** and **6**). One cavity-filling alteration, Y191W, was recognized by broadly neutralizing antibodies but exhibited only moderately reduced binding by antibody 17b, whereas two proline substitutions, Q432P and A433P, showed improved antigenic specificity. A 201C 433C double-cysteine mutant showed virtually no recognition by antibody 17b, even in the presence of CD4, but it was recognized equivalently to SOSIP.664 by antibody PGT145 and was bound even better by antibody CAP256-VRC26.09 (**Fig. 4c**). Although A433P was better recognized by broadly neutralizing antibodies than 201C 433C, the temporal stability of A433P assessed over 10 d at different temperatures (**Supplementary Data Set 2b**) was lower than that of both BG505 SOSIP.664 and 201C 433C, with 201C 433C exhibiting the

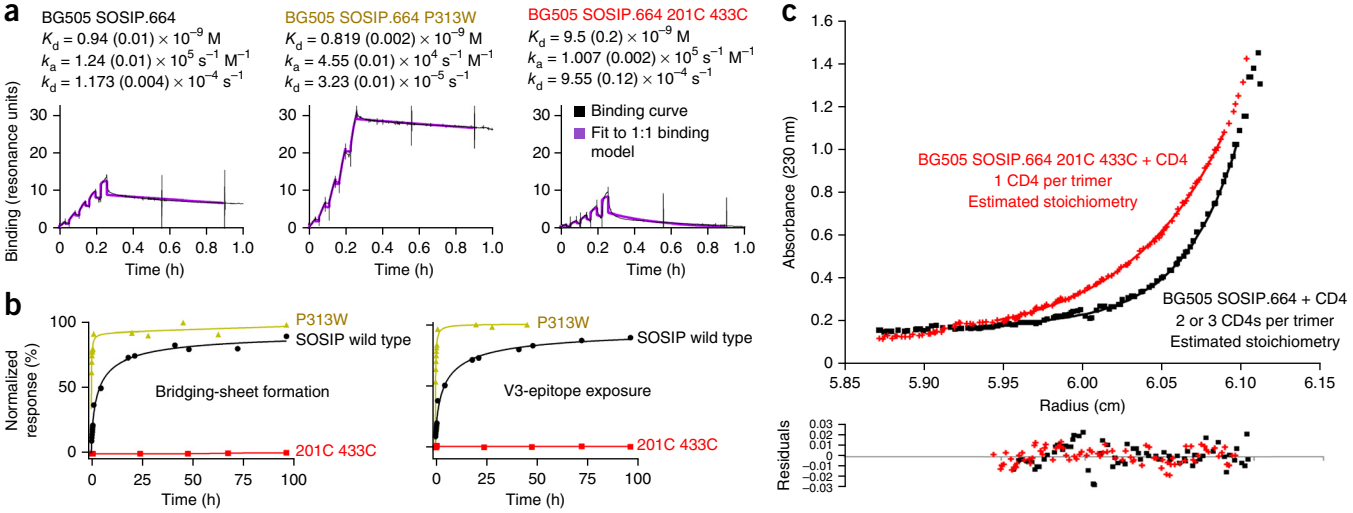

Figure 6 DS-SOSIP binds a single CD4 without the typical antigenic hallmarks of CD4 triggering. (**a**) Binding of soluble CD4 to SOSIP.664 and mutants measured by SPR with single-cycle kinetics. Values in parentheses report standard errors from fit of the data to a 1:1 Langmuir binding model. The level of binding for the P313W mutant is roughly three times higher than either wild-type SOSIP or 201C 433C. k_a and k_d represent rate of association and rate of dissociation, respectively. (**b**) Time course of CD4 activation of HIV-1 Env, as measured by SPR. To initiate the time course, CD4 was mixed with HIV-1 Env at time point 0 and, after incubation (time shown on *x* axis), was assessed by SPR for interaction with antibody (*y* axis). Left, binding to antibody 17b, which recognizes a bridging-sheet epitope; right, binding to 3074, which recognizes a V3 epitope. (**c**) Sedimentation equilibrium analytical ultracentrifugation measurements of BG505 SOSIP.664 and the 201C 433C variant in the presence of excess two-domain soluble CD4. Stoichiometry for both two-domain and four-domain CD4 as well as residual calculations are provided in **Supplementary Data Set 4**.

© 2015 Nature America, Inc. All rights reserved.

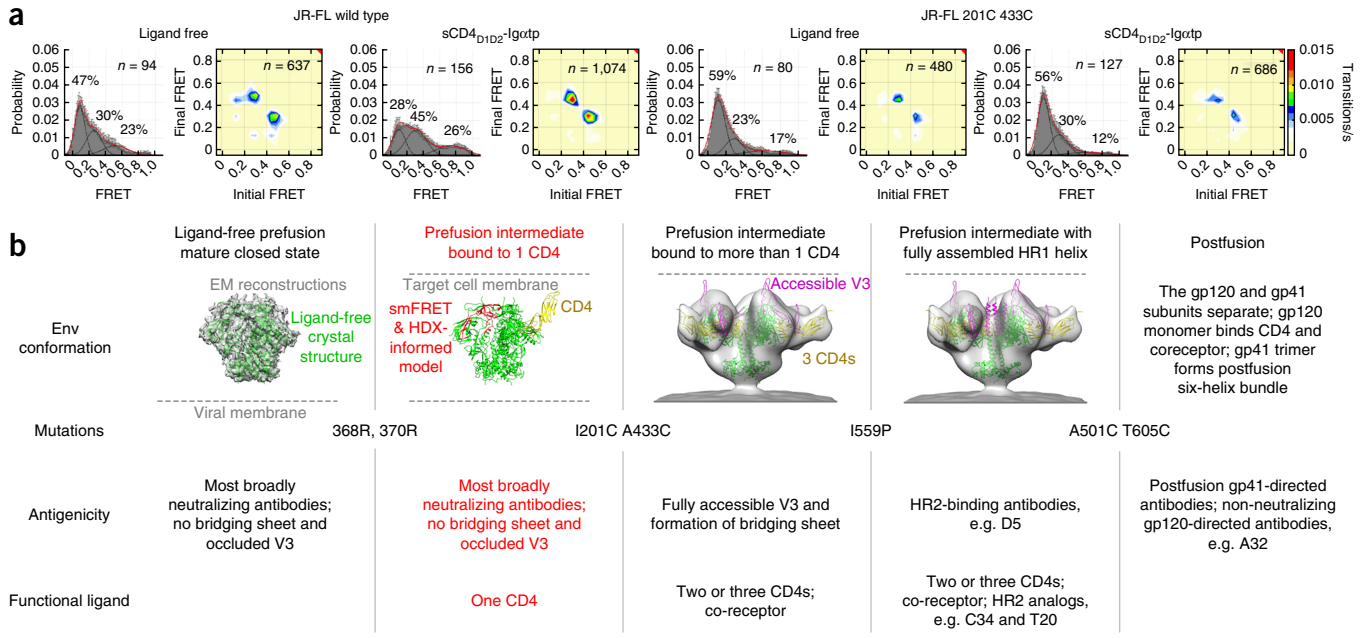

Figure 7 An asymmetric intermediate in the HIV-1–entry pathway. (**a**) smFRET of JR-FL virions with or without 201C 433C substitution. Population FRET histograms are each paired with transition density plots, which display the relative density of observed transitions. Results for both ligand-free and dodecameric CD4 ($sCD4_{D1D2}$-Igαtp) are graphed in left and right pairs, respectively. The dominance of the low-FRET state even in the presence of CD4 indicates that DS-stabilized Env remains in a closed state even when bound by CD4. (**b**) HIV-1 entry mechanism with conformation-blocking mutations, antigenicity and interactions with functional ligands. A new mechanistic state, characterized by the binding of a single molecule of CD4 with no bridging-sheet formation and reduced V3 exposure, is highlighted in red. Env-tomogram density is from refs. 13 and 60.

highest temporal stability. Notably, with the 201C 433C variant, structural compatibility with ligand-free Env correlated with antibody binding, even in the presence of CD4 (**Fig. 4d** and **Supplementary Data Set 2**). Modeling indicated that a 201C 433C disulfide is incompatible with the CD4-bound state, in which the Cαs of residues 201 and 433 are 9.4 Å apart, separated by a strand of the bridging sheet[20], and the V3 loop is fully exposed[6] (**Fig. 5a**). By contrast, the 201C 433C substitutions are expected to form a disulfide in the ligand-free closed trimer, and indeed the ligand-free BG505 SOSIP.664 201C 433C exhibited a 6.1 °C increase in thermostability (to 73.1 °C), relative to that of the parent SOSIP.664 (**Fig. 5b**), as well as increased tolerance to other physical stresses such as pH and freeze-thaw (**Fig. 5c**). These results indicated that the 201C 433C DS variant of BG505 SOSIP.664 (herein named DS-SOSIP.664) is conformationally stabilized and is not triggered by CD4.

CD4 interaction of DS-stabilized HIV-1 Env

To define the interaction of the ligand-free conformation of DS-SOSIP.664 with CD4, we used surface plasmon resonance (SPR) (**Fig. 6a**). DS-SOSIP.664 recognized CD4 with a similar on rate as that of the parent SOSIP.664 but with an off rate approximately ten-fold faster, which resulted in an approximately ten-fold reduction in K_d relative to that of SOSIP.664 (**Fig. 6a**). To test for CD4 triggering over a longer time scale, we incubated both DS-SOSIP.664 and parent SOSIP.664 for 100 h in the presence of CD4 and used SPR readout of antibody 17b or antibody 3074 to assess triggering. With the parent SOSIP.664, CD4 induced a slow transition to a state with the bridging sheet formed (time for half-maximal binding ($t_{1/2}$) of 3.3 ± 0.7 h (s.e.) for antibody 17b[43]) and the V3 loop exposed ($t_{1/2}$ of 4.2 ± 1.0 h for antibody 3074 (ref. 42)) (**Fig. 6b** and **Supplementary Data Set 3d**). With DS-SOSIP.664, we could not observe triggering by CD4 of the bridging sheet or V3 regions over the entire 100-h time course (**Fig. 6b** and **Supplementary Data Set 3d**).

To define the stoichiometry of CD4 interaction, we used sedimentation equilibrium analytical ultracentrifugation of parent and DS-SOSIP.664 variants in the presence of excess CD4. With both two-domain CD4 (**Fig. 6c**) and four-domain CD4 (**Supplementary Data Set 4**), we observed molecular weights consistent with that of the parent SOSIP.664 binding two to three CD4s and DS-SOSIP.664 binding only one CD4. DS-SOSIP.664 thus appeared to capture Env in a single-CD4–bound state.

DS-stabilized HIV-1 Env in the viral context

Because the single-CD4–bound state could be SOSIP.664 specific, we sought to assess DS-stabilized Envs in other contexts. When we placed DS mutations into functional viruses, they ablated entry (**Supplementary Data Set 5**). smFRET measurements, with donors and acceptors placed in the first and fourth variable Env loops of functional JR-FL viral spikes[28], revealed that DS mutations reduce transitions from the ground state. DS viral spikes remained primarily in the closed ground state, even in the presence of dodecameric CD4 (ref. 48) (**Fig. 7a**).

Overall, the asymmetric single-CD4–bound state—with fast off rate for CD4—appeared to be an obligatory intermediate between the ligand-free state and a more fully CD4-triggered state capable of binding multiple CD4s and co-receptor (**Fig. 7b**). In this context, we note that the high off rate of CD4 in the single-CD4–bound state, coupled with the slow transition to a 3:1 CD4/trimer stoichiometry, provides a kinetics-based molecular mechanism for the ability of primary HIV-1 isolates to resist neutralization by monomeric CD4 (ref. 49).

A new generation of DS-fixed HIV-1–Env trimeric antigens

The ligand-free Env trimer fixed in the prefusion closed conformation may be an ideal HIV-1 antigen. To obtain information on the mobility of DS-SOSIP in both ligand-free and CD4-bound states, we characterized

© 2015 Nature America, Inc. All rights reserved.

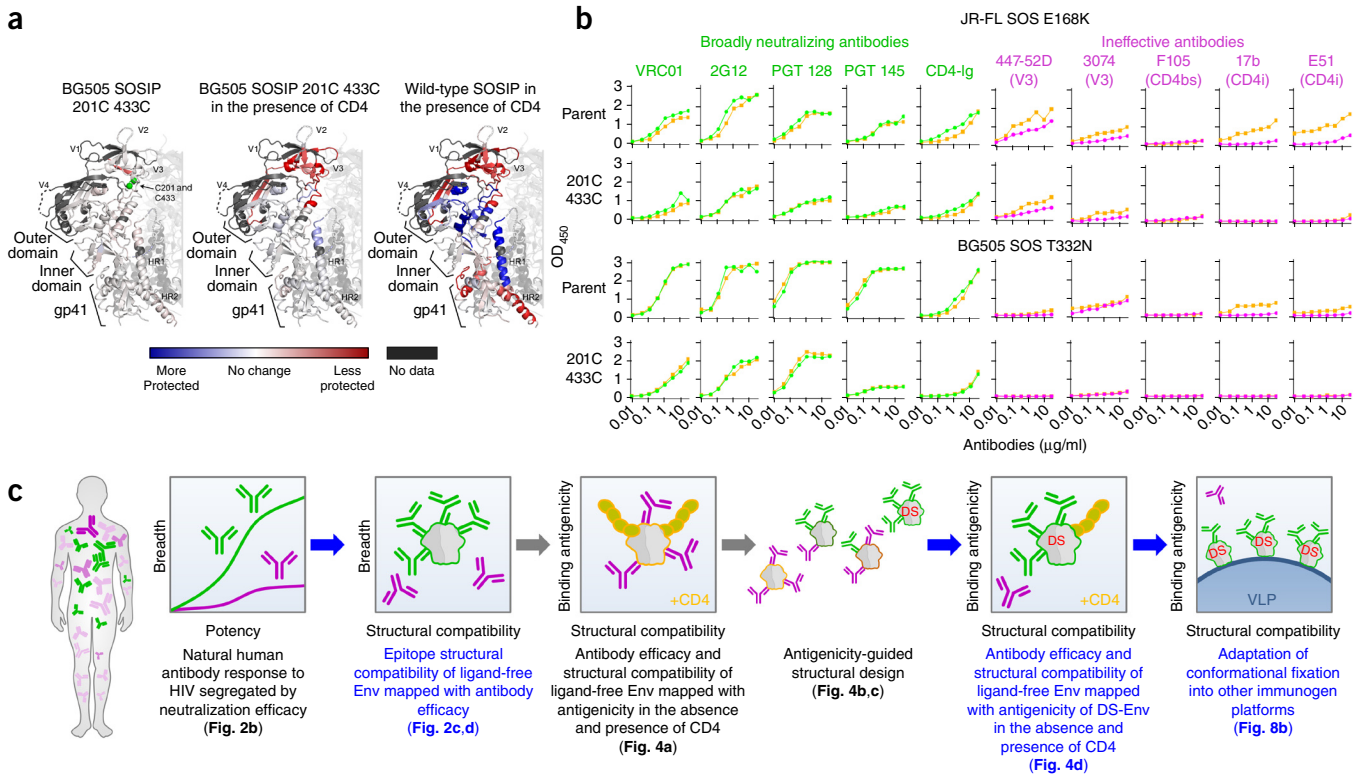

Figure 8 A new generation of conformationally fixed HIV-1–Env trimeric immunogens. (**a**) HDX characterization of conformational mobility. Changes in exchange of hydrogen/deuterium of DS-SOSIP relative to wild-type BG505 SOSIP.664 (left) or CD4-bound SOSIP relative to ligand-free SOSIP (center and right) are displayed, with regions becoming more ordered (blue) or disordered (red) shown on one lobe of the ligand-free trimer. Butterfly plots are shown in **Supplementary Fig. 7**, and full profiles are shown in **Supplementary Data Set 6**. (**b**) Antigenic characteristics of SOS virus-like particles (VLPs, comprising SOS mutant without the I559P mutation) from strain JR-FL (modified with E168K to allow binding of V1V2-directed broadly neutralizing antibodies) and strain BG505 (modified with T332N to allow binding of 2G12 antibody). Although binding of broadly neutralizing antibodies is maintained between parent and 201C 433C VLPs, the 201C 433C variant showed reduced binding of ineffective antibodies, especially in the presence of CD4. Broadly neutralizing antibodies binding are shown in green, ineffective antibodies in magenta and binding of antibodies in the presence of 2 μg/ml of sCD4 in orange. Ineffective antibodies are labeled (CD4bs, CD4-binding site; CD4i, CD4 induced; V3; V3-loop directed). OD, optical density. (**c**) Information flow of antigenicity-guided immunogen design: from human antibody response through structure and antigenicity-guided design to conformationally fixed immunogens.

© 2015 Nature America, Inc. All rights reserved.

the HDX of DS-SOSIP.664 and parent SOSIP.664 with and without CD4. Without CD4, the HDX of DS-SOSIP.664 appeared similar to that of the parent SOSIP.664 (**Fig. 8a**, **Supplementary Fig. 7** and **Supplementary Data Set 6**); with CD4, the gp120 inner domain, the bridging sheet and gp41 showed little change (**Fig. 8a**). The V2 and V3 and the stem of V1 showed a response to CD4 that was consistent with the slightly increased exposure of the V3 epitope observed by MSD-ECLIA (**Fig. 4d**), but this was substantially less than that observed for the parent SOSIP.664 (**Fig. 8a**). The CD4-bound DS-SOSIP.664 thus differs from previously observed CD4-bound states in that the typical hallmarks of CD4 induction, such as bridging-sheet formation and V3 exposure, are absent or substantially reduced.

To investigate whether the DS substitutions might serve as a general means of reducing CD4-induced transition in other Env antigens, we placed the 201C 433C and SOS mutations into HIV-1 Env expressed on the surface of enzyme-treated pseudovirions[50]. We chose two types of virions: (i) strain JR-FL, modified with E168K[51], to allow binding of V1V2-directed broadly neutralizing antibodies and (ii) strain BG505, modified with T332N[18], to allow binding of the 2G12 (ref. 52) antibody. We observed that DS-modified viral spikes resisted CD4 triggering and retained the antigenic profile of the soluble trimer for broadly neutralizing antibodies in both JR-FL and BG505 Env backgrounds (**Fig. 8b**). Overall, the results indicate that the disulfide-shackled 201C 433C variants of soluble SOSIP.664 and VLP SOS are highly desirable antigens: conformationally fixed trimers in which neutralizing epitopes are almost exclusively exposed and non-neutralizing or poorly neutralizing epitopes are hidden, even in the presence of CD4.

DISCUSSION

The path to identifying the 201C 433C DS mutant involved an information flow starting with broadly neutralizing antibodies and moving to the ligand-free Env structure and then to an analysis of its structural compatibility and binding antigenicity; this allowed us to obtain conformationally fixed antigens of desired target antigenicity (**Fig. 8c**). Such antigenicity-guided structural design may be generally applicable, and indeed an analogous design path was previously followed in the conformational stabilization of the fusion (F) glycoprotein from respiratory syncytial virus (RSV), which resulted in the production of high levels of RSV-neutralizing antibodies[44]. However, RSV F assumes primarily two conformations, prefusion[53] and postfusion[54,55], whereas HIV-1 Env can assume a multitude of conformations, including at least three prefusion states[28] and numerous conformations of separate gp120 and gp41 subunits. The conformational fixation of Env thus required analysis of antibody efficacy and antibody-induced conformation, and we formalized this with an in-depth analysis of structural compatibility. An understanding of the conformational complexity of

the HIV-1 Env, moreover, has the potential for mechanistic dividends: fixing the conformation of a particular Env entry intermediate—in this case, the ligand-free closed state—provided a means to define the mechanistic interactions of that particular state.

Unexpectedly, analysis of the DS mutant indicated an asymmetric mechanism of entry, with CD4 binding separated into two steps (**Fig. 7b**): first, recognition by one CD4 without the previously recognized antigenic hallmarks of CD4 binding such as bridging-sheet formation, and second, recognition by more than one CD4, along with exposure or formation of characteristic CD4-induced epitopes. The restricted stoichiometry of DS-SOSIP.664 is unlikely to be a consequence of steric hindrance of the binding of additional CD4 molecules by the first bound CD4; instead, the conformational change induced by the first CD4 apparently generates sufficient alterations of the Env trimer to impede the binding of a second CD4. In this context, we note that in SPR characterizations of CD4 induction (**Fig. 6b**), we observed a Hill coefficient of 0.95 ± 0.10 for the P313W mutant, which is able to rapidly engage three CD4s, and a Hill coefficient of 0.69 ± 0.06 for SOSIP.664, which displayed a $t_{1/2}$ for CD4 induction of several hours, thus suggesting negative cooperativity in which the binding of one CD4 impedes the binding of additional CD4 molecules. Although similar asymmetric or restricted binding for CD4 has been reported with other trimeric HIV-1–Env constructs[56,57], none of these other reports found binding of a single CD4 without the typical antigenic hallmarks induced by CD4, such as bridging-sheet formation[20]. In general, we believe that the single-CD4–bound trimeric state of Env is not specific to DS-SOSIP.664 but instead is an obligatory intermediate of an asymmetric entry pathway (**Fig. 7b**).

In addition to providing mechanistic insight into HIV-1 entry, antigenicity-guided conformational fixation can also improve the antigenic specificity of HIV-1–Env immunogens. We used the ligand-free HIV-1–Env trimer as a target structure because ligand-free immunogens are typically used for vaccination. In hindsight, we could have used the PGT122-35O22 antibody–bound trimer structure[14] because it is highly similar to the ligand-free structure; however, at the outset of the study, we anticipated this similarity only at the label-specific resolution of smFRET[28]. We nevertheless managed to achieve our goal: the creation of DS-Env antigens that were conformationally fixed in the vulnerable shape and were not recognized by ineffective antibodies (including those directed against V3) and were not triggered by CD4.

Even with conformational masking disabled, HIV-1 Env is additionally protected by immune evasion involving genetic variation and glycan shielding and would thus be protected by evasion mechanisms similar to those used by influenza virus hemagglutinin (**Supplementary Fig. 8**). Immunization with conformationally fixed HIV-1 Env might therefore be expected to elicit immunological responses similar to those elicited by the seasonal flu vaccine: strain-specific responses with little neutralization breadth. Indeed, this is what initial reports of immunization with BG505 SOSIP.664 have described[58]. Although an improvement over what is elicited by conformationally masked Env (for example, by gp120-subunit immunization), such strain-specific neutralization is unlikely to be generally protective. We note, however, that the immunogens in these initial reports exhibit V3-epitope exposure[18], in contrast to the V3–negatively selected DS-SOSIP described here. As a result, DS-SOSIP might be expected to induce responses that are more focused on desirable neutralizing epitopes. Altogether, because the 201C 433C DS mutation provides a means to overcome conformational masking, it should provide the basis for a new generation of vaccine antigens; however, future efforts to elicit broad HIV-1–neutralizing antibodies may require additional immunogen engineering to overcome remaining neutralization-evading mechanisms of genetic variation and glycan shielding.

METHODS

Methods and any associated references are available in the online version of the paper.

Accession codes. Coordinates and structure factors for the ligand-free BG505 SOSIP.664 trimer have been deposited in the Protein Data Bank under accession code 4ZMJ.

Note: Any Supplementary Information and Source Data files are available in the online version of the paper.

ACKNOWLEDGMENTS

We thank Y. Dai (The Scripps Research Institute) for ERV MuLV Gag plasmid, M. Murphy for SPR discussions, B. Whalen (Altravax) for the Rev plasmid, members of the Structural Biology Section and Structural Bioinformatics Core, Vaccine Research Center for discussions and comments on the manuscript and the Weill Cornell Medical College, the Academic Medical Center of the University of Amsterdam and The Scripps Research Institute HIV Vaccine Research and Design Program for their contributions to the design and validation of near-native mimicry for soluble BG505 SOSIP.664 trimers. We thank J. Baalwa, D. Ellenberger, F. Gao, B. Hahn, K. Hong, J. Kim, F. McCutchan, D. Montefiori, L. Morris, J. Overbaugh, E. Sanders-Buell, G. Shaw, R. Swanstrom, M. Thomson, S. Tovanabutra, C. Williamson and L. Zhang for contributing the HIV-1–Env plasmids used in our neutralization panel. Support for this work was provided by the Intramural Research Program of the Vaccine Research Center, National Institute of Allergy and Infectious Diseases (NIAID), US National Institutes of Health (NIH) (to J.A., A.B.M., J.R.M. and P.D.K.); the Division of AIDS, NIAID, NIH (P01-AI100151 to S.Z.-P., P01-AI104722 to L.S., R01-AI93278 to J.M.B., R21-AI100696 to W.M. and S.C.B., R21-AI112389 to K.K.L. and R33-AI84714 to J.M.B.); the US National Institutes of General Medical Sciences (P01-GM56550 to E.F., S.C.B. and W.M., R01-GM78031 to B.R.D. and R01-GM98859 to S.C.B.); the US National Institute of Heart, Lung and Blood (PO1-HL59725 to S.Z.-P.); the US National Science Foundation (MCB-1157506 to E.F.); the Bill and Melinda Gates Foundation Collaboration for AIDS Vaccine Discovery (OPP1033102 to K.K.L.); the Australian Research Council (DP130102219 to L.K.L.); the Irvington Fellows Program of the Cancer Research Program (to J.B.M.); the Department of Veterans Affairs (to S.Z.-P.); and the China Scholarship Council–Yale World Scholars (fellowship to X.M.). This project was funded in part with Federal funds to U.B. from the Frederick National Laboratory for Cancer Research, NIH, under contract HHSN261200800001E. Use of sector 22 (Southeast Region Collaborative Access team) at the Advanced Photon Source was supported by the US Department of Energy, Basic Energy Sciences, Office of Science, under contract no. W-31-109-Eng-38.

AUTHOR CONTRIBUTIONS

Y.D.K. headed the determination of the ligand-free trimer structure; M. Pancera coheaded the conformational fixation and led atomic-level investigations; P.A. coheaded the conformational fixation and led antigenic assessments; and I.S.G. headed the structural compatibility bioinformatics and designed the DS mutation. M. Pancera, T.Z., A.D. and P.D.K. contributed to structure determination; Y.D.K. and C.S. performed structural analysis; R.T.B. and M.K.L. assessed neutralization breadth; I.S.G., G.-Y.C., M.A.H., T.K., B.R.D. and L.K.L. performed structural-compatibility bioinformatics; M. Pancera, P.A., M.G.J., S.N., M.C., G.O., M. Prabhakaran, M.S., T.T., C.W., S.Z.-P. and A.B.M. performed antigenic analyses; J.G., G.B.E.S.-J., Y.Y., B.Z. and J.R.M. contributed to conformational fixation; A.H. and U.B. performed EM; M. Pancera, P.A., A.S. and E.F. performed calorimetry; Y.D.K., G.A. and L.S. performed ultracentrifugation; Y.D.K., M.G. and K.K.L. performed and analyzed HDX-MS; N.A.D.-R., S.O. and J.R.M. created and analyzed mutant virus; J.G., X.M., D.S.T., H.Z., Z.Z., J.A., J.B.M., S.C.B. and W.M. performed smFRET; P.A., M.G.J. and P.V.T. assessed physical and temporal stability; M. Pancera, E.T.C., K.O. and J.M.B. contributed VLP analysis; and I.S.G., J.S. and P.D.K. evaluated information flow. Y.D.K., M. Pancera, P.A., I.S.G. and P.D.K. assembled and wrote the paper, on which all principal investigators commented.

COMPETING FINANCIAL INTERESTS

The authors declare no competing financial interests.

© 2015 Nature America, Inc. All rights reserved.

Reprints and permissions information is available online at http://www.nature.com/reprints/index.html.

1. Starcich, B.R. *et al.* Identification and characterization of conserved and variable regions in the envelope gene of HTLV-III/LAV, the retrovirus of AIDS. *Cell* **45**, 637–648 (1986).
2. Wei, X. *et al.* Antibody neutralization and escape by HIV-1. *Nature* **422**, 307–312 (2003).
3. Chen, L. *et al.* Structural basis of immune evasion at the site of CD4 attachment on HIV-1 gp120. *Science* **326**, 1123–1127 (2009).
4. Kwong, P.D. *et al.* HIV-1 evades antibody-mediated neutralization through conformational masking of receptor-binding sites. *Nature* **420**, 678–682 (2002).
5. Fouts, T.R., Binley, J.M., Trkola, A., Robinson, J.E. & Moore, J.P. Neutralization of the human immunodeficiency virus type 1 primary isolate JR-FL by human monoclonal antibodies correlates with antibody binding to the oligomeric form of the envelope glycoprotein complex. *J. Virol.* **71**, 2779–2785 (1997).
6. Huang, C.C. *et al.* Structure of a V3-containing HIV-1 gp120 core. *Science* **310**, 1025–1028 (2005).
7. Weiss, R.A. *et al.* Neutralization of human T-lymphotropic virus type III by sera of AIDS and AIDS-risk patients. *Nature* **316**, 69–72 (1985).
8. Bures, R. *et al.* Immunization with recombinant canarypox vectors expressing membrane- anchored glycoprotein 120 followed by glycoprotein 160 boosting fails to generate antibodies that neutralize R5 primary isolates of human immunodeficiency virus type 1. *AIDS Res. Hum. Retroviruses* **16**, 2019–2035 (2000).
9. Flynn, N.M. *et al.* Placebo-controlled phase 3 trial of a recombinant glycoprotein 120 vaccine to prevent HIV-1 infection. *J. Infect. Dis.* **191**, 654–665 (2005).
10. Liu, J., Bartesaghi, A., Borgnia, M.J., Sapiro, G. & Subramaniam, S. Molecular architecture of native HIV-1 gp120 trimers. *Nature* **455**, 109–113 (2008).
11. Bartesaghi, A., Merk, A., Borgnia, M.J., Milne, J.L. & Subramaniam, S. Prefusion structure of trimeric HIV-1 envelope glycoprotein determined by cryo-electron microscopy. *Nat. Struct. Mol. Biol.* **20**, 1352–1357 (2013).
12. Julien, J.P. *et al.* Crystal structure of a soluble cleaved HIV-1 envelope trimer. *Science* **342**, 1477–1483 (2013).
13. Lyumkis, D. *et al.* Cryo-EM structure of a fully glycosylated soluble cleaved HIV-1 envelope trimer. *Science* **342**, 1484–1490 (2013).
14. Pancera, M. *et al.* Structure and immune recognition of trimeric pre-fusion HIV-1 Env. *Nature* **514**, 455–461 (2014).
15. Wu, X. *et al.* Neutralization escape variants of human immunodeficiency virus type 1 are transmitted from mother to infant. *J. Virol.* **80**, 835–844 (2006).
16. Binley, J.M. *et al.* A recombinant human immunodeficiency virus type 1 envelope glycoprotein complex stabilized by an intermolecular disulfide bond between the gp120 and gp41 subunits is an antigenic mimic of the trimeric virion-associated structure. *J. Virol.* **74**, 627–643 (2000).
17. Sanders, R.W. *et al.* Stabilization of the soluble, cleaved, trimeric form of the envelope glycoprotein complex of human immunodeficiency virus type 1. *J. Virol.* **76**, 8875–8889 (2002).
18. Sanders, R.W. *et al.* A next-generation cleaved, soluble HIV-1 Env trimer, BG505 SOSIP.664 gp140, expresses multiple epitopes for broadly neutralizing but not non-neutralizing antibodies. *PLoS Pathog.* **9**, e1003618 (2013).
19. Kwon, Y.D. *et al.* Unliganded HIV-1 gp120 core structures assume the CD4-bound conformation with regulation by quaternary interactions and variable loops. *Proc. Natl. Acad. Sci. USA* **109**, 5663–5668 (2012).
20. Kwong, P.D. *et al.* Structure of an HIV gp120 envelope glycoprotein in complex with the CD4 receptor and a neutralizing human antibody. *Nature* **393**, 648–659 (1998).
21. Zhou, T. *et al.* Structural definition of a conserved neutralization epitope on HIV-1 gp120. *Nature* **445**, 732–737 (2007).
22. Zhou, T. *et al.* Structural basis for broad and potent neutralization of HIV-1 by antibody VRC01. *Science* **329**, 811–817 (2010).
23. Pejchal, R. *et al.* A potent and broad neutralizing antibody recognizes and penetrates the HIV glycan shield. *Science* **334**, 1097–1103 (2011).
24. Scharf, L. *et al.* Antibody 8ANC195 reveals a site of broad vulnerability on the HIV-1 envelope spike. *Cell Reports* **7**, 785–795 (2014).
25. Wyatt, R. & Sodroski, J. The HIV-1 envelope glycoproteins: fusogens, antigens, and immunogens. *Science* **280**, 1884–1888 (1998).
26. Chan, D.C., Fass, D., Berger, J.M. & Kim, P.S. Core structure of gp41 from the HIV envelope glycoprotein. *Cell* **89**, 263–273 (1997).
27. Weissenhorn, W., Dessen, A., Harrison, S.C., Skehel, J.J. & Wiley, D.C. Atomic structure of the ectodomain from HIV-1 gp41. *Nature* **387**, 426–430 (1997).
28. Munro, J.B. *et al.* Conformational dynamics of single HIV-1 envelope trimers on the surface of native virions. *Science* **346**, 759–763 (2014).
29. Guttman, M. *et al.* Antibody potency relates to the ability to recognize the closed, pre-fusion form of HIV Env. *Nat. Commun.* **6**, 6144 (2015).
30. Jancarik, J.K.S.-H. Sparse matrix sampling: a screening method for crystallization of proteins. *J. Appl. Crystallogr.* **24**, 409–411 (1991).
31. Majeed, S. *et al.* Enhancing protein crystallization through precipitant synergy. *Structure* **11**, 1061–1070 (2003).
32. Adams, P.D. *et al.* Recent developments in the PHENIX software for automated crystallographic structure determination. *J. Synchrotron Radiat.* **11**, 53–55 (2004).
33. Korber, B.T., Foley, B.T., Kuiken, C.L., Pillai, S.K. & Sodroski, J.G. in *Human Retroviruses and AIDS 1998: a Compilation and Analysis of Nucleic Acid and Amino Acid Sequences* Part III (eds. Korber, B., Kuiken, C.L., Foley, B., Hahn, B., McCutchan, F., Mellors, J.W. & Sodroski, J.) 102–111 (Los Alamos National Laboratory, 1998).
34. Burton, D.R. *et al.* Efficient neutralization of primary isolates of HIV-1 by a recombinant human monoclonal antibody. *Science* **266**, 1024–1027 (1994).
35. Huang, J. *et al.* Broad and potent neutralization of HIV-1 by a human antibody that binds the gp41–gp120 interface. *Nature* **515**, 138–142 (2014).
36. Walker, L.M. *et al.* Broad neutralization coverage of HIV by multiple highly potent antibodies. *Nature* **477**, 466–470 (2011).
37. Zolla-Pazner, S. *et al.* The cross-clade neutralizing activity of a human monoclonal antibody is determined by the GPGR V3 motif of HIV type 1. *AIDS Res. Hum. Retroviruses* **20**, 1254–1258 (2004).
38. Liao, H.-X. *et al.* Co-evolution of a broadly neutralizing HIV-1 antibody and founder virus. *Nature* **496**, 469–476 (2013).
39. Guenaga, J. *et al.* Well-ordered trimeric HIV-1 subtype B and C soluble spike mimetics generated by negative selection display native-like properties. *PLoS Pathog.* **11**, e1004570 (2015).
40. Mbah, H.A. *et al.* Effect of soluble CD4 on exposure of epitopes on primary, intact, native human immunodeficiency virus type 1 virions of different genetic clades. *J. Virol.* **75**, 7785–7788 (2001).
41. Stanfield, R.L., Gorny, M.K., Williams, C., Zolla-Pazner, S. & Wilson, I.A. Structural rationale for the broad neutralization of HIV-1 by human monoclonal antibody 447–52D. *Structure* **12**, 193–204 (2004).
42. Jiang, X. *et al.* Conserved structural elements in the V3 crown of HIV-1 gp120. *Nat. Struct. Mol. Biol.* **17**, 955–961 (2010).
43. Thali, M. *et al.* Characterization of conserved human immunodeficiency virus type 1 gp120 neutralization epitopes exposed upon gp120–CD4 binding. *J. Virol.* **67**, 3978–3988 (1993).
44. McLellan, J.S. *et al.* Structure-based design of a fusion glycoprotein vaccine for respiratory syncytial virus. *Science* **342**, 592–598 (2013).
45. Wu, X. *et al.* Rational design of envelope identifies broadly neutralizing human monoclonal antibodies to HIV-1. *Science* **329**, 856–861 (2010).
46. Doria-Rose, N.A. *et al.* Developmental pathway for potent V1V2-directed HIV-neutralizing antibodies. *Nature* **509**, 55–62 (2014).
47. Posner, M.R., Cavacini, L.A., Emes, C.L., Power, J. & Byrn, R. Neutralization of HIV-1 by F105, a human monoclonal antibody to the CD4 binding site of gp120. *J. Acquir. Immune Defic. Syndr.* **6**, 7–14 (1993).
48. Arthos, J. *et al.* Biochemical and biological characterization of a dodecameric CD4-Ig fusion protein: implications for therapeutic and vaccine strategies. *J. Biol. Chem.* **277**, 11456–11464 (2002).
49. Daar, E.S. & Ho, D.D. Relative resistance of primary HIV-1 isolates to neutralization by soluble CD4. *Am. J. Med.* **90**, 22S–26S (1991).
50. Crooks, E.T., Tong, T., Osawa, K. & Binley, J.M. Enzyme digests eliminate nonfunctional Env from HIV-1 particle surfaces, leaving native Env trimers intact and viral infectivity unaffected. *J. Virol.* **85**, 5825–5839 (2011).
51. Tong, T., Crooks, E.T., Osawa, K. & Binley, J.M. HIV-1 virus-like particles bearing pure env trimers expose neutralizing epitopes but occlude nonneutralizing epitopes. *J. Virol.* **86**, 3574–3587 (2012).
52. Trkola, A. *et al.* Human monoclonal antibody 2G12 defines a distinctive neutralization epitope on the gp120 glycoprotein of human immunodeficiency virus type 1. *J. Virol.* **70**, 1100–1108 (1996).
53. McLellan, J.S. *et al.* Structure of RSV fusion glycoprotein trimer bound to a prefusion-specific neutralizing antibody. *Science* **340**, 1113–1117 (2013).
54. McLellan, J.S., Yang, Y., Graham, B.S. & Kwong, P.D. Structure of respiratory syncytial virus fusion glycoprotein in the postfusion conformation reveals preservation of neutralizing epitopes. *J. Virol.* **85**, 7788–7796 (2011).
55. Swanson, K.A. *et al.* Structural basis for immunization with postfusion respiratory syncytial virus fusion F glycoprotein (RSV F) to elicit high neutralizing antibody titers. *Proc. Natl. Acad. Sci. USA* **108**, 9619–9624 (2011).
56. Kovacs, J.M. *et al.* Stable, uncleaved HIV-1 envelope glycoprotein gp140 forms a tightly folded trimer with a native-like structure. *Proc. Natl. Acad. Sci. USA* **111**, 18542–18547 (2014).
57. Pancera, M. *et al.* Soluble mimetics of human immunodeficiency virus type 1 viral spikes produced by replacement of the native trimerization domain with a heterologous trimerization motif: characterization and ligand binding analysis. *J. Virol.* **79**, 9954–9969 (2005).
58. Sanders, R.W. *et al.* HIV-1 neutralizing antibodies induced by native-like envelope trimers. *Science* doi:10.1126/science.aac4223 (18 June 2015).
59. McLellan, J.S. *et al.* Structure of HIV-1 gp120 V1/V2 domain with broadly neutralizing antibody PG9. *Nature* **480**, 336–343 (2011).
60. Tran, E.E. *et al.* Structural mechanism of trimeric HIV-1 envelope glycoprotein activation. *PLoS Pathog.* **8**, e1002797 (2012).

© 2015 Nature America, Inc. All rights reserved.

ONLINE METHODS

BG505 SOSIP.664 expression, purification and deglycosylation. BG505 SSOIP.664 trimer was produced in HEK 293 GnTI$^{-/-}$ cells via transient transfection of the BG505 SOSIP–expressing plasmid with furin and purified as described previously, over a 2G12 affinity column[12,14,18] (additional details, including transient transfection in 96-well plates in **Supplementary Note**). The cell line was purchased from ATCC (cat. no. CRL-3022) and was authenticated and checked for mycoplasma contamination by the vendor. The eluted protein was then dialyzed against PBS and set for deglycosylation reaction at 37 °C in reaction buffer containing 1 mM EDTA, 150 mM NaCl, protease-inhibitor cocktail (Roche), 17,000 units of Endo H per ml and 50 mM sodium acetate, pH 5.8. The deglycosylated BG505 SOSIP was further purified with a Superdex 200 16/60 (GE Healthcare) column in buffer containing 5 mM HEPES, pH 7.5, 150 mM NaCl and 0.02% NaN_3. The peak corresponding to trimeric HIV-1 Env was identified, pooled and concentrated to ~10 mg/ml with an Amicon Ultra-15 centrifugal filter (MWCO 50,000, Millipore) and screened for crystallization. Similarly purified 'crystallization-grade' samples were also used for HDX experiments.

For most antigenicity and stability analyses, after trimers were purified by affinity chromatography and gel filtration over a Superdex 200 16/60 (GE Healthcare) column in buffer containing 5 mM HEPES, pH 7.5, 150 mM NaCl and 0.02% NaN_3, they were subjected to negative selection[39]. This generally involved a V3 antibody 447-52D (PDB 4M1D[61]) affinity column to remove aberrant trimer species. However, for select antigenic analyses (for example, **Fig. 4a**,**d**), an additional column comprising a cocktail of V3-directed antibodies, 1006-15D, 2219, 2557, 2558, 3074 and 50.1 (PDB 3MLW[42], 2B0S[62], 3MLS[42], 3UJI[63], 3MLX[42], 1GGI[64], respectively), was used (**Fig. 3**, **Supplementary Data Set 1** and **Supplementary Note**).

Crystallization screening. Deglycosylated BG505 SOSIP.664 was screened for crystallization with 572 conditions in Hampton, Wizard and Precipitant Synergy[31] screens with a Cartesian Honeybee crystallization robot, as described previously[59], and a mosquito robot with 0.1 µl of reservoir solution and 0.1 µl of protein solution. Crystals suitable for structural determination were obtained robotically in 26% PEG 400, 3.2% PEG 3350 and 0.1 M sodium acetate, pH 5.5. Crystals were cryoprotected in a solution containing 30% glycerol, 30% PEG 400, 4% PEG 3350 and 0.1 M sodium acetate, pH 5.5, and were flash frozen in liquid nitrogen. Data were collected at a wavelength of 1.00 Å at the SER-CAT beamline ID-22 (Advanced Photon Source, Argonne National Laboratory).

X-ray data collection, structure solution and model building. Diffraction data were processed with the HKL2000 suite[65]. The data were corrected for anisotropy with the anisotropy server http://services.mbi.ucla.edu/anisoscale/ with truncations to 3.7 Å, 3.7 Å and 3.3 Å along the a, b and c axes, respectively. Structure solution was obtained with Phaser with 35O22- and PGT122-bound BG505 SOSIP.664 (PDB 4TVP[14]) as a search model. Refinement was carried out with Phenix[32]. Model building was carried out with Coot[66]. Data collection and refinement statistics are shown in **Table 1**.

Structural analyses involving residue-specific properties. To estimate the degree of structural flexibility in the ligand-free HIV-1 trimer, we determined the average Cα r.m.s. deviation distance for each residue position in the ligand-free trimer structure (**Fig. 2d**,**e**). The average Cα r.m.s. deviation distance served as a proxy for structural plasticity and was computed between corresponding residues after optimal superimposition onto a set of 98 structures from the Protein Data Bank (PDB)[67]. Each domain of the ligand-free trimer was considered separately and superimposed onto the set of structures with either the program TM-align[68] or single-value decomposition (SVD). To obtain the correct registry between corresponding residues, structural superimpositions were guided by amino acid sequence alignments when necessary. A total of 63 monomeric structures were used for superimpositions involving the gp120 domain (**Supplementary Table 2**). To generate **Figure 2a** (left), we used five representative gp120 structures; ligand-free clade A/E HIV-1 gp120 core$_e$ (PDB 3TGT)[19], b12-bound gp120 (PDB 2NY7)[21], b13-bound gp120 (PB 3IDX)[3], F105-bound gp120 (PB 3HI1)[3] and VRC01-bound gp120 (PDB 3NGB)[69] structures. For the gp41 domain, we used a total of 35 structures from the PDB that included hexameric bundles as well as disordered peptides (**Supplementary Table 2**).

To understand the dynamic properties of ligand-free BG505 SOSIP.664, qualitative exchange profiles for observable peptides of SOSIP.664 after 3 s were extracted from individual HDX-MS exchange plots[70]. The average exchange values (0–75%) were substituted in the *B*-factor field for the observed peptides of closed, ligand-free BG505 SOSIP.664 coordinates and displayed within PyMOL (http://www.pymol.org/) (**Supplementary Figs. 1g** and **2g**). Peptides not observed in the deuterium-exchange experiment as well as peptides with missing electron density were excluded from the analysis.

Other residue-specific properties were calculated and are shown in **Supplementary Table 1**. These included residue depth[71], solvent-accessible surface area (SASA) (NACCESS program; S. Hubbard and J. Thornton (University College London)), sequence variability and hydrophobicity. Residue sequence variability was computed as the Shannon entropy for each residue position on the basis of a representative set of 3,943 HIV-1 strains (**Supplementary Figs. 1e** and **2e**). The electrostatic-potential surfaces were generated with GRASP[72]. The Pearson correlation coefficient and associated *P* values (computed with two-tailed *t* test) were computed with the statistical package R. Residue-level and surface property analyses were carried out with coordinates that differed slightly from those deposited in the PDB (r.m.s. deviation of the analyzed coordinates differed by 0.02 Å for regions compared, and *B* factors were identical).

Assessment of antibody-functionality on a panel of 170 diverse HIV-1 isolates. Neutralization was measured with single-round-of-infection HIV-1–Env pseudoviruses and TZM-bl target cells, as described previously[73]. Neutralization curves were fit by nonlinear regression with a five-parameter Hill-slope equation. The 50% and 80% inhibitory concentrations (IC_{50} and IC_{80}) were reported as the antibody concentrations required to inhibit infection by 50% and 80%, respectively. The following antibodies were tested for HIV-1 neutralization efficacy: 17b[20], 48D[74], E51 (ref. 75), 35O22 (ref. 76), 447-52D[61], 8ANC195 (ref. 77), VRC01 (ref. 45), b12 (ref. 21), b13 (ref. 3), CH103 (ref. 78), F105 (ref. 3), PG9 (ref. 36), PG16 (ref. 36), PGT145 (ref. 36), PGT128 (ref. 36), PGT135 (ref. 36) and 2G12 (ref. 79).

Computation of antibody-epitope r.m.s. deviation, volume overlap and epitope presence. HIV-1–specific antibody–antigen complex structures were compiled from the PDB, and antibodies were defined as broadly or poorly/non neutralizing, according to published or in-house neutralization data of diverse viral strains[80]. Antibodies that were deemed to have insufficient evidence for being classified as broadly or poorly/non neutralizing were excluded from the analysis. A single antibody representative was included in the analysis in cases in which multiple antibody clonal relatives were found. The epitope residues for each antibody were defined on the basis of the respective antibody–antigen complex crystal structures, with an antigen residue being defined as an epitope residue if any of its heavy atoms were within 5.5 Å of any antibody heavy atom. To compute the r.m.s. deviation between the epitope residues in the antibody–antigen complex structure and the same residues in the ligand-free trimer structure, first the epitope residues from the complex structure were aligned to the ligand-free trimer structure with the align function in PyMOL, and then the Cα r.m.s. deviation of the epitope residues was calculated. To remove outlier residues, the top and bottom 10% of the Cα deviations were removed from the r.m.s. deviation calculation. To calculate the volume overlap between a given antibody and the ligand-free trimer structure, the alignment from above was used to compute the overlap volume between the antibody from the complex structure and the ligand-free trimer structure with the phase_volCalc utility from Schrödinger (http://www.schrodinger.com/). An antibody epitope was considered to be present in the ligand-free trimer structure if at least 70% of the epitope residues as defined by the antibody–antigen complex structure were also present in the ligand-free trimer structure. For mapping the per-residue r.m.s. deviation computation onto the ligand-free trimer structure, residues part of any antibody epitope (including epitopes with less than 70% total residues present) were included in the analysis; if a given residue was part of more than one antibody epitope, the highest r.m.s. deviation value for that residue among all epitopes was used. Antibody-volume-overlap values were mapped onto the ligand-free trimer structure for all residues part of the epitope for the given antibody; if a residue was part of more than one antibody epitope, then the lowest volume overlap for that residue among all epitopes was used. Correlations of structural properties with neutralization and/or binding data were computed with the Spearman correlation coefficient with two-tailed *P* values.

© 2015 Nature America, Inc. All rights reserved.

doi:10.1038/nsmb.3051

Structural compatibility analysis. For a given antibody, the antigenic structural compatibility (ASC) score with the HIV-1–Env ligand-free prefusion trimer structure was computed on the basis of comparison to a structure of the antibody bound to an Env-derived antigen (for example, gp120 core or V3 peptide). ASC scores were computed on a 0–1 scale with the following variables: (i) The fraction *f* of epitope residues (as defined by the structure of the antibody complex) exposed to solvent in the ligand-free trimer structure was computed. A residue was considered to be accessible to solvent if its solvent-accessible surface area (SASA) was at least half its SASA in the respective antibody complex structure, and *f* was set to 0 if <70% of epitope residues were present in the antigen. (ii) A resolution estimate *r* was used, such that Cα r.m.s. deviations *d* below $r = 2$ were not penalized in the scores. (iii) The volume-overlap values were used to define a volume-overlap factor *v* that is equal to 1 for overlap below 200 Å^3 and is equal to 0 for overlap over 1,000 Å^3, and decays linearly in between. Intuitively, the ligand-free trimer structure is expected to be structurally compatible with an antibody if *f* and *v* are high and if the r.m.s. deviation *d* is low, because such conditions would indicate similarity between the ligand-free trimer structure and the Env conformation in the antibody complex. Thus, the ASC score for each antibody with the ligand-free trimer was defined by the formula: $fv\exp(-0.5\max(0,d-r))$.

Antigenic analysis of BG505 SOSIP.664 and mutants by MSD-ECLIA and ELISA. Standard 96-well bare MULTI-ARRAY Meso Scale Discovery (MSD) Plates (MSD, cat. no. L15XA-3) were coated with a panel of HIV-neutralizing (VRC01 (ref. 45), b12 (ref. 21), PGT121 (ref. 36), PGT128 (ref. 36), 2G12 (ref. 79), PGT145 (ref. 36), VRC26.09 (ref. 81), 35O22 (ref. 76) and 8ANC195 (ref. 77)), non-neutralizing monoclonal antibodies (F105 (ref. 3), 1.5e[82], 17b[20] and 447-52D[61]) and noncognate antibodies (anti-influenza antibodies CR9114 (ref. 83) and CR8020 (ref. 84), as well as anti-RSV antibodies palivizumab[85], D25 (ref. 53) and 5C4 (ref. 53), in duplicates (30 µL/well) at a concentration of 10 µg/mL, diluted in 1× PBS, and the plates were incubated overnight at 4 °C. The following day, plates were washed (wash buffer: 0.05% Tween-20 + 1× PBS) and blocked with 150 µL of blocking buffer (5% (w/v) MSD blocker A (MSD, cat. no. R93BA-4)) and incubated for 1 h on a vibrational shaker (Heidolph TITRAMAX 100, cat. no. 544-11200-00) at 650 r.p.m. All the incubations were performed at room temperature, except the coating step. During the incubation, BG505 SOSIP trimer was titrated down in serial two-fold dilutions starting at 4 µg/mL concentration of the trimer in assay diluent (1% (w/v) MSD blocker A + 0.05% Tween-20). After the incubation with blocking buffer was complete, the plates were washed, and the diluted trimer was transferred (25 µl/well) to the MSD plates and incubated for 2 h on the vibrational shaker at 650 r.p.m. For soluble CD4 (sCD4) induction, trimer was preincubated with sCD4 at a constant molar concentration of 1 µM for 1 h before being added to the MSD plate. After the 2-h incubation with trimer, the plates were washed again and secondary detection was performed with MSD Sulfotag-labeled D7324 antibody. (Before the assay, D7324 antibody was labeled with MSD Sulfotag (MSD, cat. no. R91AN-1) at a conjugation ratio of 1:15 D7324/Sulfotag, which was diluted in assay diluent at 5 µg/mL and was added to the plates (25 µL/well) and incubated for 1 h on the vibrational shaker at 650 r.p.m. The plates were washed and read with 1× read buffer (MSD Read Buffer T (4×); cat. no. R92TC-2) on an MSD Sector Imager 2400.

ELISA methods are described in **Supplementary Note**.

Surface plasmon resonance analysis. Affinities and kinetics of binding to BG505 SOSIP.664 soluble trimer and its mutants were assessed by surface plasmon resonance on a Biacore T-200 (GE Healthcare) at 20 °C with buffer HBS-EP+ (10 mM HEPES, pH 7.4, 150 mM NaCl, 3 mM EDTA and 0.05% surfactant P-20). Affinities for mAbs PGT121 and 2G12 were taken from published values[18].

To assess binding of trimer to sCD4, single-cycle kinetics analyses were carried out. First, ~2,000 RU of antibody 2G12 was immobilized on two flow cells. Next, 200 nM of trimer was injected on the sample flow cell. Finally, sCD4 at five concentrations (100 nM, 50 nM, 25 nM, 12.5 nM and 6.25 nM) was injected incrementally in a single cycle, starting from the lowest concentration; this was followed by a dissociation phase of 30 min. Blank sensorgrams were obtained by injection of the same volume of HBS-EP+ buffer in place of sCD4. Sensorgrams of the concentration series were corrected with corresponding blank curves and fitted globally with Biacore T200 evaluation software with a 1:1 Langmuir model of binding.

For determination of the time course of CD4 activation of the soluble trimers, 17b IgG, 3074 IgG and 2G12 IgG were captured on three separate flow cells of a CM5 chip immobilized with ~10,000 RU of mouse anti-human Fc antibody (described above). One flow cell immobilized with ~10,000 RU of mouse anti-human Fc antibody was used as reference flow cell. Trimers were incubated in four-fold molar excess of sCD4, and samples were injected at different time points. Blank sensorgrams were obtained by injection of the same volume of HBS-EP+ buffer in place of trimer and were subtracted from reference-subtracted sensorgrams obtained with trimer samples. Binding levels in double-referenced sensorgrams were measured 40 s after sample injection. To measure any change in the trimer samples upon incubation, ligand-free trimers were injected before and 72 h after the start of the experiment. (Additional SPR assay methods are described in **Supplementary Note**.)

Biolayer interferometry analysis. A fortéBio HTX instrument was used to measure affinities of SOSIP.664 and DS-SOSIP.664 to a panel of HIV-1–Env reactive antibodies at 30 °C (details in **Supplementary Note**).

Negative-stain electron microscopy. Negative-stain EM samples were diluted to about 0.03 mg/ml, adsorbed to a freshly glow-discharged carbon-film grid for 15 s and stained with 0.7% uranyl formate. Images were collected semiautomatically with SerialEM[86] on an FEI Tecnai T20 with a 2,000 × 2,000 Eagle CCD camera at a pixel size of 0.22 nm/px. Particles were picked automatically, and reference-free 2D classification was performed in EMAN2 (ref. 87).

Differential scanning calorimetry. The heat capacity of BG505 SOSIP.664 and DS-SOSIP.664 was measured as a function of temperature with a high-precision differential scanning VP-DSC microcalorimeter (GE Healthcare/Microcal). The samples were extensively dialyzed against PBS, pH 7.4, and then degassed to avoid the formation of bubbles in the calorimetric cells. Thermal denaturation scans were conducted from 10 to 100 °C at a rate of 1 °C/min. The protein concentration was about 0.3 mg/mL.

Analytical ultracentrifugation equilibrium measurements. Analytical ultracentrifugation (AUC) equilibrium experiments were performed at 15 °C, with a Beckman XL-A/I ultracentrifuge equipped with a Ti60An rotor (additional details in **Supplementary Note**).

Hydrogen/deuterium exchange (HDX). The hydrogen/deuterium exchange rates for BG505 SOSIP.664 and the DS-SOSIP.664 both alone and in the presence of CD4 were assessed. Complexes with soluble CD4 (D1D2) were formed by overnight incubation with a nine-fold molar excess of ligand (relative to trimer). Proteins (10 µg) were diluted ten-fold into deuterated PBS buffer and incubated at room temperature. Aliquots removed after 3 s, 1 min, 30 min and 20 h were quenched by mixture with an equal volume of cold 200 mM Tris-2-carboxyethyl phosphine (TCEP), and 0.2% formic acid, final pH 2.5. The samples were subsequently digested with pepsin (at 0.15 mg/mL) for 5 min on ice, flash frozen in liquid nitrogen and stored at −80 °C. For LC-MS analysis, samples were thawed on ice for 5 min and manually injected onto a Waters BEH 1.7 µm 1.2 × 5 mm trap column (Waters) flowing 0.1% TFA at 200 µL/min. After 3 min of washing, the peptides were resolved over a Hypersil 1 × 50 mm 2.1 µm C18 column (Thermo Scientific) with a gradient of 15 to 40% B in 8 min (A, 0.05% TFA and 5% ACN; B, 0.05% TFA and 80% ACN). Eluted peptides were analyzed with a Waters Synapt Q-TOF mass spectrometer. Peptide identification and exchange analysis were as described previously[70].

Neutralization of viral entry. The point mutations were introduced into full-length Env clone BG505.W6M.C2 (ref. 15) in expression vector pcDNA3.1/V5-His-TOPO (Invitrogen). Pseudotyped, single-round-of-entry virus was produced as described in Shu *et al.*[88]. Briefly, plasmid DNA was used to transfect HEK 293T cells along with an envelope-deficient HIV-1 subtype A proviral plasmid, SG3dEnv[89], to generate pseudotyped viral particles. Serial dilutions of the pseudovirus stocks were added to TZMbl reporter cells, and 2 d later the activity of the luciferase reporter gene in infected cells was assessed with a Luciferase Assay kit (Promega) and measured in a luminometer; activity was reported as relative light units (RLU).

smFRET on JR-FL viral spikes. smFRET experiments were performed as previously described[28]. Briefly, HEK 293 cells were transfected at a 40:1 ratio of wild-type

© 2015 Nature America, Inc. All rights reserved.

HIV-$1_{JR\text{-}FL}$ or HIV-$1_{JR\text{-}FL\ 201C\ 433C}$ Env to dually V1-Q3/V4-A1 tagged Env, and pNL4-3 Δenv ΔRT was additionally present (details in **Supplementary Note**).

Assessment of physical stability. To assess physical stability of the prefusion, closed conformation of SOSIP.664 and DS-SOSIP.664, we subjected the proteins to a variety of pharmaceutically relevant stresses such as extreme pH, high temperature and repeated freeze/thaw cycles. The physical stability of treated BG505 SOSIP and 201C 433C proteins was reported as the fraction of binding retained to the quaternary-specific V1V2-directed antibody CAP256-VRC26.09 with a fortéBio Octet HTX instrument. To assess physical stability over time, the trimers were incubated at 4 °C, 20 °C, 37 °C and 42 °C, aliquots were taken at different time points and binding to CAP256-VRC26.09 was measured (details in **Supplementary Note**).

Virus-like particles. Virus-like particles containing protease-purified Env trimers were prepared as previously described[50,51,90], and ELISAs on these VLPs were performed as previously described[51]. Briefly, Immulon II plates (Thermo) were coated overnight at 4 °C with VLPs at 20 times their concentration in transfection supernatants. Wells were washed with PBS and then blocked with 4% bovine serum albumin/10% FBS in PBS. Various biotinylated monoclonal antibodies (biotinylated with sulfo-NHS-Xbiotin, Thermo), and CD4-IgG2 (NIH AIDS Reagent Program, cat. no. 11780) were then titrated in the presence or absence of a fixed concentration of 2 μg/ml soluble CD4. Alkaline phosphatase conjugated to streptavidin (Vector Laboratories; to detect biotinylated mAbs) or anti-Fc (Accurate; to detect CD4-IgG2) and SigmaFAST *p*-nitrophenyl phosphate tablets (Sigma) were then used to detect binding. Plates were read at 405 nm.

61. Killikelly, A. *et al.* Thermodynamic signatures of the antigen binding site of mAb 447–52D targeting the third variable region of HIV-1 gp120. *Biochemistry* **52**, 6249–6257 (2013).
62. Stanfield, R.L., Gorny, M.K., Zolla-Pazner, S. & Wilson, I.A. Crystal structures of human immunodeficiency virus type 1 (HIV-1) neutralizing antibody 2219 in complex with three different V3 peptides reveal a new binding mode for HIV-1 cross-reactivity. *J. Virol.* **80**, 6093–6105 (2006).
63. Gorny, M.K. *et al.* Human anti-V3 HIV-1 monoclonal antibodies encoded by the VH5–51/VL lambda genes define a conserved antigenic structure. *PLoS ONE* **6**, e27780 (2011).
64. Rini, J.M. *et al.* Crystal structure of a human immunodeficiency virus type 1 neutralizing antibody, 50.1, in complex with its V3 loop peptide antigen. *Proc. Natl. Acad. Sci. USA* **90**, 6325–6329 (1993).
65. Otwinowski, Z. & Minor, W. Processing of X-ray diffraction data collected in oscillation mode. *Methods Enzymol.* **276**, 307–326 (1997).
66. Emsley, P. & Cowtan, K. Coot: model-building tools for molecular graphics. *Acta Crystallogr. D Biol. Crystallogr.* **60**, 2126–2132 (2004).
67. Bernstein, F.C. *et al.* The Protein Data Bank: a computer-based archival file for macromolecular structures. *J. Mol. Biol.* **112**, 535–542 (1977).
68. Zhang, Y. & Skolnick, J. TM-align: a protein structure alignment algorithm based on the TM-score. *Nucleic Acids Res.* **33**, 2302–2309 (2005).
69. Pancera, M. *et al.* Structure of HIV-1 gp120 with gp41-interactive region reveals layered envelope architecture and basis of conformational mobility. *Proc. Natl. Acad. Sci. USA* **107**, 1166–1171 (2010).
70. Guttman, M. *et al.* CD4-induced activation in a soluble HIV-1 Env trimer. *Structure* **22**, 974–984 (2014).
71. Sanner, M.F., Olson, A.J. & Spehner, J.C. Reduced surface: an efficient way to compute molecular surfaces. *Biopolymers* **38**, 305–320 (1996).
72. Nicholls, A., Sharp, K.A. & Honig, B. Protein folding and association: insights from the interfacial and thermodynamic properties of hydrocarbons. *Proteins* **11**, 281–296 (1991).
73. Sarzotti-Kelsoe, M. *et al.* Optimization and validation of the TZM-bl assay for standardized assessments of neutralizing antibodies against HIV-1. *J. Immunol. Methods* **409**, 131–146 (2014).
74. Huang, C.C. *et al.* Structural basis of tyrosine sulfation and VH-gene usage in antibodies that recognize the HIV type 1 coreceptor-binding site on gp120. *Proc. Natl. Acad. Sci. USA* **101**, 2706–2711 (2004).
75. Xiang, S.H. *et al.* Epitope mapping and characterization of a novel CD4-induced human monoclonal antibody capable of neutralizing primary HIV-1 strains. *Virology* **315**, 124–134 (2003).
76. Huang, J. *et al.* Broad and potent HIV-1 neutralization by a human antibody that binds the gp41-gp120 interface. *Nature* **515**, 138–142 (2014).
77. Scheid, J.F. *et al.* Broad diversity of neutralizing antibodies isolated from memory B cells in HIV-infected individuals. *Nature* **458**, 636–640 (2009).
78. Liao, H.X. *et al.* Co-evolution of a broadly neutralizing HIV-1 antibody and founder virus. *Nature* **496**, 469–476 (2013).
79. Calarese, D.A. *et al.* Antibody domain exchange is an immunological solution to carbohydrate cluster recognition. *Science* **300**, 2065–2071 (2003).
80. Georgiev, I.S. *et al.* Delineating antibody recognition in polyclonal sera from patterns of HIV-1 isolate neutralization. *Science* **340**, 751–756 (2013).
81. Doria-Rose, N.A. *et al.* Developmental pathway for potent V1V2-directed HIV-neutralizing antibodies. *Nature* **509**, 55–62 (2014).
82. Seaman, M.S. *et al.* Tiered categorization of a diverse panel of HIV-1 Env pseudoviruses for assessment of neutralizing antibodies. *J. Virol.* **84**, 1439–1452 (2010).
83. Dreyfus, C. *et al.* Highly conserved protective epitopes on influenza B viruses. *Science* **337**, 1343–1348 (2012).
84. Tharakaraman, K., Subramanian, V., Cain, D., Sasisekharan, V. & Sasisekharan, R. Broadly neutralizing influenza hemagglutinin stem-specific antibody CR8020 targets residues that are prone to escape due to host selection pressure. *Cell Host Microbe* **15**, 644–651 (2014).
85. Palivizumab, a humanized respiratory syncytial virus monoclonal antibody, reduces hospitalization from respiratory syncytial virus infection in high-risk infants. The IMpact-RSV Study Group. *Pediatrics* **102**, 531–537 (1998).
86. Mastronarde, D.N. Automated electron microscope tomography using robust prediction of specimen movements. *J. Struct. Biol.* **152**, 36–51 (2005).
87. Tang, G. *et al.* EMAN2: an extensible image processing suite for electron microscopy. *J. Struct. Biol.* **157**, 38–46 (2007).
88. Shu, Y. *et al.* Efficient protein boosting after plasmid DNA or recombinant adenovirus immunization with HIV-1 vaccine constructs. *Vaccine* **25**, 1398–1408 (2007).
89. Wei, X. *et al.* Emergence of resistant human immunodeficiency virus type 1 in patients receiving fusion inhibitor (T-20) monotherapy. *Antimicrob. Agents Chemother.* **46**, 1896–1905 (2002).
90. Tong, T., Osawa, K., Robinson, J.E., Crooks, E.T. & Binley, J.M. Topological analysis of HIV-1 glycoproteins expressed *in situ* on virus surfaces reveals tighter packing but greater conformational flexibility than for soluble gp120. *J. Virol.* **87**, 9233–9249 (2013).

© 2015 Nature America, Inc. All rights reserved.
npg